Energy Conversion and Management 268 (2022) 116030

Contents lists available at ScienceDirect

Energy Conversion and Management

journal homepage: www.elsevier.com/locate/enconman

Products of catalytic oxidative coupling of methane to improve thermal efficiency in natural gas engines

Seokwon Cho [a], Hyewon Lee [a], Ying Lin [a], Satbir Singh [b], William F. Northrop [a,*]

[a] Department of Mechanical Engineering, University of Minnesota, Minneapolis, MN 55455, USA
[b] Mechanical Engineering Department, Carnegie Mellon University, Pittsburgh, PA 15213, USA

ARTICLE INFO

Keywords:
Natural gas
Oxidative coupling of methane
Combustion properties
Internal combustion engines

ABSTRACT

Pretreating natural gas using catalytic oxidative coupling of methane (OCM) produces ethylene and ethane, both species that increase fuel reactivity, thus increasing the potential to expand the operability range of highly efficient compression ignition combustion in natural gas engines. This paper presents the first experimental results on the impact of OCM product species on engine thermal efficiency and operability range. In the work, a benchtop experiment was conducted to generate a product species distribution from OCM over a Sr/La_2O_3 catalyst. A computational study using known chemical mechanisms was then employed to investigate the laminar flame speed and ignition delay of the OCM-modified fuel. Finally, engine experiments in both spark-ignition and compression-ignition combustion modes were carried out using a variable compression ratio single-cylinder engine. Results from the benchtop catalyst experiments showed that practical fuel conversion for single-pass OCM resulted in 18 % methane conversion, 60 % C_2 selectivity, and 10.8 % C_2 yield at a molar C/O ratio of 6. After determining realistic fuel blending ratios for engine operation, the numerical simulation results showed that fuel reactivity and ignition delay improved compared to with methane alone, while laminar flame speed decreased due to higher dilution from the presence of inert OCM products. Engine experimental results confirmed that OCM products have an advantage in CI mode due to reduced ignition delay time. The CI operating range was widely expanded, and approximately 9.9% thermal efficiency gain was achieved. By contrast, efficiency in SI mode was reduced when using OCM products due to an increase in combustion duration and retarded combustion phasing.

1. Introduction

Global demand for natural gas (NG) energy has increased in the past decade due to its lower carbon intensity compared to other fossil fuels and the development of efficient extraction techniques [1,2]. As a fuel for internal combustion engines, NG has a clear advantage over conventional fuels in reducing harmful emissions like carbon dioxide and particulate matter [3]. Due to its inherent knock resistance, it also allows a higher compression ratio in spark ignition (SI) engines resulting in higher thermal efficiency. Methane, the highest concentration species in NG, is more molecularly stable than other hydrocarbons due to its lack of carbon-carbon bonds, giving NG low ignition reactivity. This feature renders NG an unattractive choice for compression-ignition (CI) engines [1,4,5], thus limiting further improvements in NG engine efficiency.

Numerous studies have investigated the usefulness and applicability of NG in internal combustion engines through modeling and experiments. Various published studies have focused on the impacts of injection strategies [6–8], ignition enhancement [9,10], increased

Abbreviations: 0D, zero-dimensional; 3D, Three-dimensional; aBDC, After bottom dead center; aTDC, After top dead center; bTDC, Before top dead center; bBDC, Before bottom dead center; C/O, Carbon-to-oxygen ratio; CA, Crank angle; CA50, Crank angle at mass burn point 50%; CAI, Controlled autoignition; CFD, Computational fluid dynamics; CFR, Cooperative fuel research; COV, Covariance; DME, Dimethyl ether; EVC, Exhaust valve closing; EVO, Exhaust valve opening; GC, Gas chromatography; GHSV, Gas hourly space velocity; gIMEP, Gross indicated mean effective pressure; gISFC, Gross indicated specific fuel consumption; gITE, Gross indicated thermal efficiency; HCCI, Homogeneous charge compression ignition; HRR, Heat release rate; IDT, Ignition delay time; IVC, Intake valve closing; IVO, Intake valve opening; LFS, Laminar flame speed; LHV, Lower heating value; MBT, Maximum brake torque; MFC, Mass flow controller; mIDT, Merit in ignition delay time; NG, Natural gas; NTC, Negative temperature coefficient; OCM, Oxidative coupling of methane; POx, Partial oxidation; P-T, Pressure-Temperature; RI, Ringing intensity; SI, Spark-ignition; SLPM, Standard liter per minute; TDC, Top dead center; WOT, Wide-open throttle.

* Corresponding author.
E-mail address: wnorthro@umn.edu (W.F. Northrop).

https://doi.org/10.1016/j.enconman.2022.116030
Received 8 June 2022; Received in revised form 11 July 2022; Accepted 18 July 2022
Available online 26 July 2022

compression ratio [11], lean-burn [12,13], boosting [14,15], and exhaust gas recirculation [15,16]. Advanced combustion modes, including homogeneous charge compression ignition (HCCI) with NG, have been demonstrated [11,17–19] in attempts to overcome low fuel reactivity and realize higher engine efficiency. Generally, impractically high intake pressure and temperature are required to successfully enable stable CI ignition with methane or NG.

Previous studies have reported that higher carbon number fuel additives such as propane can be advantageous in facilitating stable CI combustion in engines by slightly increasing the reactivity of the fuel mixture [18]. Converting a small portion of the incoming methane in NG to more reactive species is a potential concept for enabling CI over a wider range of operations. Partial oxidation produces syngas species (CO and H_2) and has been explored for fuels including methane [20–22], methane-dimethyl ether (DME) mixtures [23], and DME alone [24]. Although the H_2 found in syngas has a relatively high laminar flame speed compared to hydrocarbons, it also has high autoignition resistivity, limiting its advantage for CI operation. Further issues with decreased volumetric efficiency due to dilution and heating and reduced lower heating value (LHV) must still be addressed for partial oxidation (POx) to be a viable fuel pre-treatment option [25].

An alternative fuel pre-treatment approach is oxidative coupling of methane (OCM), which converts methane to higher molecular weight hydrocarbons rather than lighter syngas species. OCM first gained attention as an alternative for industrial synthesis of ethylene from NG for polymer synthesis and several other important industrial processes. Reactions 1–3 show the processes and enthalpy changes of stoichiometric combustion, POx, and OCM, with air as the oxidant. Complete combustion (Reaction (1)) is highly exothermic and produces products with no extractable chemical enthalpy. POx (Reaction (2)) is less exothermic and produces syngas, as previously discussed. The OCM reaction (Reaction (3)) produces C_2 species (ethane, ethylene, and acetylene) at the same stoichiometry as POx. Desired products of the OCM reaction are higher in reactivity and lower heating values than H_2 and CO. The OCM reaction proceeds in the presence of a catalyst at temperatures ranging from 700 to 900 °C [26].

$$CH_4 + 2(O_2 + 3.76N_2) \rightarrow CO_2 + 2H_2O + 7.52N_2 \Delta H^\circ_{298K} = -802.56 kJ/mol_{CH_4} \quad \text{(R1)}$$

$$CH_4 + 1/2(O_2 + 3.76N_2) \rightarrow CO + 2H_2 + 1.88N_2 \Delta H^\circ_{298K} = -35.9 kJ/mol_{CH_4} \quad \text{(R2)}$$

$$CH_4 + 1/2(O_2 + 3.76N_2) \rightarrow 1/2C_2H_4 + H_2O + 1.88N_2 \Delta H^\circ_{298K} = -140.98 kJ/mol_{CH_4} \quad \text{(R3)}$$

Oxidative coupling of methane is a heterogeneous catalytic reaction first discovered by Keller and Bhasin in the 1980s [27]. Although the exact gas and surface phase mechanism for OCM is still under investigation, the general mechanism is understood to be initialized by methane activation via H-abstraction on a charged surface oxygen site, followed by gas phase reaction of the methyl radicals to produce ethane, and finalized by gas-phase dehydrogenation of ethane to ethylene [28,29]. A schematic of one proposed mechanism is shown in Fig. 1.

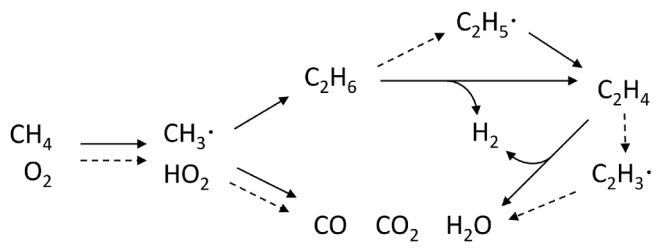

Fig. 1. Conceptual diagram of the OCM mechanism (modified from [28]). Solid arrows indicate pathways of gas phase reactions, and dashed arrows show those of surface reactions.

The desirable reaction pathway for OCM, as shown in Reaction (3), produces ethylene, although ethane and other unselective products are also generated in practical reactors. Several side reactions occur that produce undesirable inert species like CO_x and H_2O. To maximize C_2 yield and minimize undesirable products, it is important to choose appropriate operating conditions. The methane (carbon) to oxygen ratio (C/O) in the reactants is an important parameter for OCM operation. While the stoichiometric C/O for combustion is 2, the C/O for OCM generally ranges from 4 to 8. A low C/O ratio (i.e., where oxygen concentration is relatively high) lowers selectivity to C_2 products as oxygen facilitates oxidation of not only methane but also the produced C_2 hydrocarbons [30–32]. This additional oxidation, occurring at C/O <6, can cause hotspots in the catalyst C/O that can cause irreversible deactivation of the catalyst, further reducing conversion and selectivity.

Early theoretical and experimental studies sought to determine the best OCM catalyst in terms of C_2 yield and selectivity to ethylene. Desirable physical characteristics for an OCM catalyst include moderate to high basicity for efficient oxygen adsorption allowing efficient H-abstraction, and high thermal stability for a long catalyst life [33–36]. In past decades, Mg/O, La_2O_3, and $Mn/Na_2WO_4/SiO_2$ catalysts have shown good performance in terms of C_2 yield, especially when modified with metals and metal oxides such as Ca, La, or Mn_xO_y [34,37–43]. In this work, lanthanum oxide doped with strontium, Sr/La_2O_3, was used as the OCM catalyst. This combination of a rare earth metal oxide and an alkaline earth metal has been shown to be active in OCM at low temperatures (<650 °C) [44].

OCM has been investigated intensively since its discovery, but the commercialization of this process at an industrial scale has yet to be realized [45,46]. One of the main hurdles is the trade-off relationship between methane conversion and C_2 selectivity limiting the yield of valuable products. It is commonly agreed that a C_2 yield of 30–35 % is needed to make OCM commercially viable, a target met by only a few demonstration reactors reported in the publicly available literature [30,47,48].

While OCM for ethylene production requires high methane conversion and ethylene yield, OCM for engine fuel pre-treatment is less stringent because only a small concentration of added C_2 products, including ethylene and ethane, can have a significant impact on fuel mixture reactivity. In the early 2000s, Langille et al. [49,50] suggested the use of OCM to convert methane into molecules with higher ignition reactivity for combustion applications and showed, both experimentally and through simulations, that the addition of C_2 species enhanced the ignition characteristics of lean methane-air combustion. They simulated both a packed bed reactor and a membrane reactor. Model-estimated products were used to determine the ignition temperature of fuel-oxidizer mixture impinging on a hot solid surface. Results showed that as the mole fraction of ethylene and ethane in the fuel increased, ignition temperature decreased significantly. Beyond these initial studies, no further work has directly integrated an OCM reactor with an engine to demonstrate its potential to lower ignition energy, lower dilute or lean operation, or allow advanced combustion modes such as low-temperature combustion.

This work presents the first published study investigating the feasibility of using OCM as a fuel pre-treatment technique to increase fuel reactivity, and consequently the thermal efficiency, of internal combustion engines. In the study, research was conducted to investigate the trade-off of increased reactivity of OCM- modified fuel against the loss of heating value of the fuel, and to demonstrate the viability of this novel concept. A benchtop OCM reactor experiment was conducted to determine a realistic fuel blend for engine applications, followed by a numerical simulation study of the laminar flame speed and ignition delay of practical fuel blends to better understand their impact on combustion. Finally, single-cylinder engine experiments were conducted to elucidate the effect of pre-treated fuel mixtures on thermal efficiency in spark-ignition (SI) and compression-ignition (CI) combustion modes.

2. Methodology

2.1. Benchtop catalyst experimental setup

Fig. 2 provides a schematic of the experimental setup used for the benchtop experiment to investigate the feasibility of NG fuel pre-treatment using OCM. The catalyst used was Sr/La_2O_3 particles, sieved in the range of 0.5–1 mm and provided by Johnson Matthey. A 20 mm quartz tube reactor was packed with 1 g of the Sr/La_2O_3 catalyst. Although particulate catalysts are not ideal for practical engine reactors, the purpose of the benchtop reactor tests was to generate realistic OCM product distributions that could be used to study the effects on engine combustion. Quartz wool plugs were placed on each side of the catalyst bed. The downstream section of the catalyst bed was filled with inert alumina pellets to keep the bed centered in the quartz tube reactor. The reactor was placed in a tube furnace to heat the catalyst bed to the desired temperature. The flow rates of the reactant gases (methane, air, and nitrogen) were individually controlled by Alicat Scientific mass flow controllers (MFCs). A K-type thermocouple was placed at the end of the catalyst bed to monitor the temperature. The product gas was directed to a container placed in an ice bath to condense water prior to sampling and gas chromatography (GC) analysis. An Inficon Micro-GC equipped with Molesive and Rt U-band columns was used to analyze the concentration of the dry product stream.

The inlet gas mixture was prepared with a molar C/O between 6 and 8 and 10% dilution with nitrogen, and the total flow rate was 1.5 standard liters per minute (SLPM), resulting in a gas hourly space velocity (GHSV) of 72,000 hr^{-1}. At the beginning of the experiment, pure nitrogen was supplied to heat the reactor to 600 °C. When a steady state was reached in the catalyst, nitrogen was replaced by the methane and air mixture to start the catalytic reaction. An inlet mixture with C/O = 8 was introduced first and then changed to C/O = 6 later in the experiment to test catalyst performance at two different C/O ratios.

Methane conversion, C_2 selectivity, and C_2 yield were used to assess OCM performance. Methane conversion refers to how much inlet methane was converted to OCM products. The calculation of methane conversion of the reactor is shown in Eq. (1):

$$X_{CH_4} = \frac{\dot{n}_{CH_4,in} - \dot{n}_{CH_4,out}}{\dot{n}_{CH_4,in}} \quad (1)$$

where n is the molar flow rate, and subscripts *in* and *out* refer to inlet and outlet, respectively. C_2 selectivity (Eq. (2)) describes how much of the converted methane became desired products, and C_2 yield (Eq. (3)) indicates the percentage of C_2 products produced compared to the theoretical maximum.

$$S_{C_{2+}} = \frac{2\left(\dot{n}_{C_2H_6,out} + \dot{n}_{C_2H_4,out} + \dot{n}_{C_2H_2,out}\right) + 3(\dot{n}_{C_3H_8,out} + \dot{n}_{C_3H_6,out})}{X_{CH_4} * \dot{n}_{CH_4,in}} \quad (2)$$

$$Y_{C_{2+}} = X_{CH_4} \bullet S_{C_{2+}} \quad (3)$$

2.2. Numerical simulation of combustion properties

2.2.1. Laminar flame speed

Laminar flame speed (LFS) is an intrinsic property of fuel that is a function of the unburnt mixture composition, temperature, and pressure [51–54]. It is a very important input parameter when calculating the turbulent flame speed, which greatly affects combustion duration [54], particularly during flame propagation in internal combustion engines. LFS is especially relevant for the cooperative fuel research (CFR) engine used in this study due to the engine's less favorable design for turbulence. In addition, operation in SI mode in this engine is more likely to entail premixed combustion than in a regular direct-injection SI engine because the feed fuel is in a gaseous state. Thus, laminar flame speed is the key factor in determining combustion behavior and can provide insight into how a modified fuel affects combustion.

This study used three mechanisms to calculate LFS, namely, GRI 3.0 [55], ARIES82 [56] and Aramco3.0 [57]. GRI 3.0 is a widely used and relatively simple mechanism containing 53 species and 325 reactions [55]. Aramco 3.0 [57] is a comprehensive mechanism consisting of 581 species and 3037 reactions; it is believed to be the most accurate but is computationally expensive. ARIES82 is a reduced mechanism suggested by Mohr et al. [56] and has 82 species and 519 reactions.

The LFS computations were carried out by the High-Performance Computing systems in the Minnesota Supercomputing Institute at the University of Minnesota. The calculations were done under various conditions associated with engine operation using Cantera 2.4.0 [58] and Python 3.7 with in-house code that enabled multiprocessing computation. A one-dimensional freely propagating premixed flame object (*FreeFlame*) was used in the calculation, where initial grid size was 0.05 cm, tolerance for steady state was 10^{-5} (relative) and 10^{-13} (absolute), tolerance for transient was 10^{-4} (relative) and 10^{-13} (absolute), and maximum time step count was 700.

2.2.2. Ignition delay time

Ignition delay time (IDT) is defined as the period between a mixture's exposure to a combustible environment and its ignition. In engine combustion, IDT is generally defined as the time interval between the start of fuel injection to the start of combustion [59], or the intake valve closing to the start of combustion. The latter is more commonly used for a premixed combustion engine.

Previous studies reported that adding a small amount of low molecular weight hydrocarbons to NG combustion led to shorter IDT [49,60–62]. Fraser et al. [63] specifically looked at the effect of ethane to methane-air combustion in a simulated diesel environment using a combustion vessel and found that it slightly decreased the IDT[63]. Other studies also found that adding C_2 species decreased IDT under premixed combustion conditions [49,50,64]. The decrease was mainly due to the lower oxidation activation energy of ethane (40 kcal/mol) compared to that of pure methane (46 kcal/mol) [64,65]. The addition of C_2 species was also found to [18].

In this study, Aramco3.0 [57] mechanism was used, and the

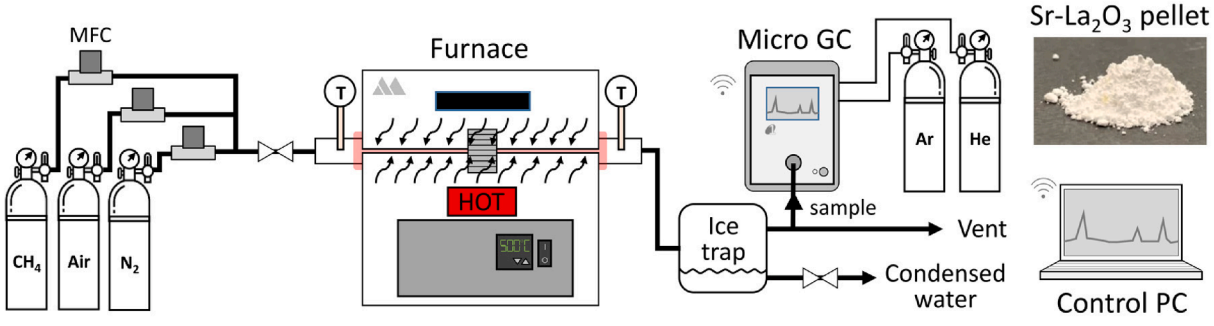

Fig. 2. Schematic diagram of the OCM catalyst bench-top experiment.

computation was conducted in MATLAB to solve the following equation of constant volume reactor simulation [66] using a variable-step, variable-order solver (*ode15s*):

$$\frac{dT}{dt} = \frac{1}{mC_v}\left[-\sum_{species}\left\{ \dot{w} \bullet V \bullet \left(\frac{h}{RT} - 1\right)\overline{R} \right\} \right] T \tag{4}$$

where $\dot{w}$ is the net production rate, h is the specific enthalpy, P is the cylinder pressure, R is the gas constant, and $\overline{R}$ is the universal gas constant. Thermodynamic and chemical properties were imported from the Cantera 2.4.0 libraries and mechanisms. IDT was defined as the timing at which the mixture temperature increased 300 K from the initial state. This criterion is not recommended for lean burn of fuels that have a significant multi-stage ignition process, due to possible misleading results due to dilution and negative temperature coefficient (NTC) behaviors; typically, a criterion of maximum temperature rise is recommended. However, the ignition processes of the fuels used in this study are very straightforward without NTC.

Because modified fuel contains not only C_2 species but also other species such as nitrogen and carbon dioxide that can also affect IDT, a new parameter, *merit in IDT* (mIDT) is introduced to quantify the benefits of fuel modification on IDT. mDIT (Eq (5)) is defined as the ratio of the IDT of pure methane to the IDT of a fuel of interest:

$$IDTmerit(mIDT) = \frac{\tau_{CH_4}}{\tau_{fuel}} \tag{5}$$

The higher the mIDT, the more the modified fuel improves ignition characteristics.

2.3. Experimental engine setup

2.3.1. Engine experimental setup

A Waukesha CFR engine was commissioned at Thomas E. Murphy Engine Research Laboratory at the University of Minnesota for experimental investigation. CFR facilities are the standard engine setup to measure motor octane number (ASTM D2700) and research octane number (ASTM D2699). Since the original configuration of the engine was designed for liquid fuel supply, it was retrofitted with gaseous fuel supply system to test methane-based fuels for this study. Table 1 shows detailed specifications of the engine.

The compression ratio was varied by changing the engine cylinder's squish height. A very subtle change in the squish height results in a significant change in the pressure profile during compression, and this substantially affects the IDT of the mixture. Thus, the compression ratio was confirmed before firing the engine by matching results from an in-house GT-power engine model as well as a three-dimensional (3D) computational fluid dynamics (CFD) simulation using a model provided by the Argonne National Laboratory [6768]. The motoring peak pressure was maintained within ± 0.2 bar of the reference profile, which was confirmed before starting the combustion. The range of variable compression ratio was 4 to 18 in the engine spec, and compression ratios of 9 and 18 were used in this study.

Table 1
Salient features of the CFR engine.

Displacement volume [cm^3]	611.7
Bore [mm]	82.55
Stroke [mm]	114.3
Connecting rod [mm]	254
Piston offset [mm]	0
Crank radius [mm]	57.2
Compression ratio	Variable (4 to 23)
Number of valves	2
Maximum valve lift [mm]	6
Intake valve	180° shroud with anti-rotation pin
IVO/IVC (@1mm)	10 CA aTDC/34CA aBDC
Exhaust valve	No shroud with rotator assembly
EVO/EVC (@1mm)	40CA bBDC/15CA aTDC

Fig. 3 illustrates the configuration of the experimental system. A three-phase AC reluctance-type synchronous power absorption motor was used for the dynamometer, and the engine was belt-driven by the motor. Intake air was supplied by a scroll-type air compressor on the mezzanine. The supplied air was dried, and its pressure was regulated before the air was supplied to a mass flow controller. Both the intake and exhaust sides have plenums to stabilize the air flow to achieve high-fidelity steady-state data. The intake air pressure was measured using a pressure transducer (Omega PX419-100A5V) located in the intake manifold, and the pressure was controlled within ± 0.005 bar during the experiment. The intake charge temperature was controlled within ± 0.5 K using a heater coil (Omega AHF-10120) downstream of the intake plenum by taking feedback input from a K-type thermocouple located at 100 mm before the intake valve. The gaseous fuel was supplied upstream of the intake manifold to develop a sufficient premixed condition.

An integrated evaporative cooling system was used for engine cooling. The vaporized water floats up to the coolant tower where it condenses. The condensed water sinks back to the coolant jacket, creating natural convection within the loop. The coolant temperature was measured at the point where the coolant moves back into the coolant jacket and was carefully maintained at 98.5 ± 0.5 °C throughout the experimental campaign. Engine oil was supplied with an internal gear-driven pump, and the pressure was kept constant at 3.5 bar of gauge pressure using a pressure regulating system.

The knock meter of the CFR engine was retrofitted with a Kistler 6125B in-cylinder pressure transducer with an adapter to flush-mount the sensor to the chamber. The pressure signal was amplified using a Kistler type 5010 amplifier. Combustion was monitored in real-time, and the data was logged during the experiments using an in-house combustion analyzing system. The system was programmed with National Instrument (NI) LabVIEW. An NI PXI-8115 controller mounted in an NI PXI-1042 chassis and an NI PXI-6251 multifunction DAQ were used for the hardware. The data logger was designed to save the data in TDMS format with a maximum resolution of 300 consecutive cycle data in 0.1 crank angle (CA). For high repeatability, the experiments required, in addition to precise control of the intake and coolant temperatures, data for a high number of cycles. Thus 200 cycle data collection was repeated ten times to achieve a total of two thousand cycles and was saved using a buffer. The low-frequency data such as mass flow rates and temperatures were all 3-minute ensemble-averaged and logged.

The engine controller was established using an in-house LabView code utilizing an NI cRIO-9074 chassis and several modules (NI 9264, 9205, 9211, 9201, and 9401) as operating hardware. Four MFCs were used to regulate the flows of CH_4, CO_2, N_2, and OCM product mixture. The system also controlled the spark timing using a TTL signal and production type power transistor, and the control resolution was 0.1 CA using a 3600-teeth encoder.

2.3.2. Engine operating conditions

Table 2 shows the engine operating conditions. The engine speed was fixed at 900 rpm. The engine experiments were conducted in both SI and CI modes. SI mode was tested at compression ratio 9, and an intake pressure of 0.865 bar at part-load and 1 bar at full-load. The spark timing was 20 CA before top dead center (bTDC) at part-load and 23 CA bTDC at full-load. The equivalence ratio was set to one (stoichiometric) throughout the SI mode test, assuming full utilization of a three-way catalyst. Due to the poor ignitability of the baseline fuel (pure methane) and the slow initial flame propagation speed of the CFR engine, the intake temperature was increased up to 200 °C during the experiments. The CI mode experiments were conducted under compression ratio 18, WOT condition. A lean-burn mixture was introduced to the engine to maximize the OCM-modified fuel's advantage in IDT as well as to decrease the ringing intensity (RI) of the combustion. During the experiment, the equivalence ratio was calculated using carbon balance. At a given equivalence ratio, the ratio of flow rates of

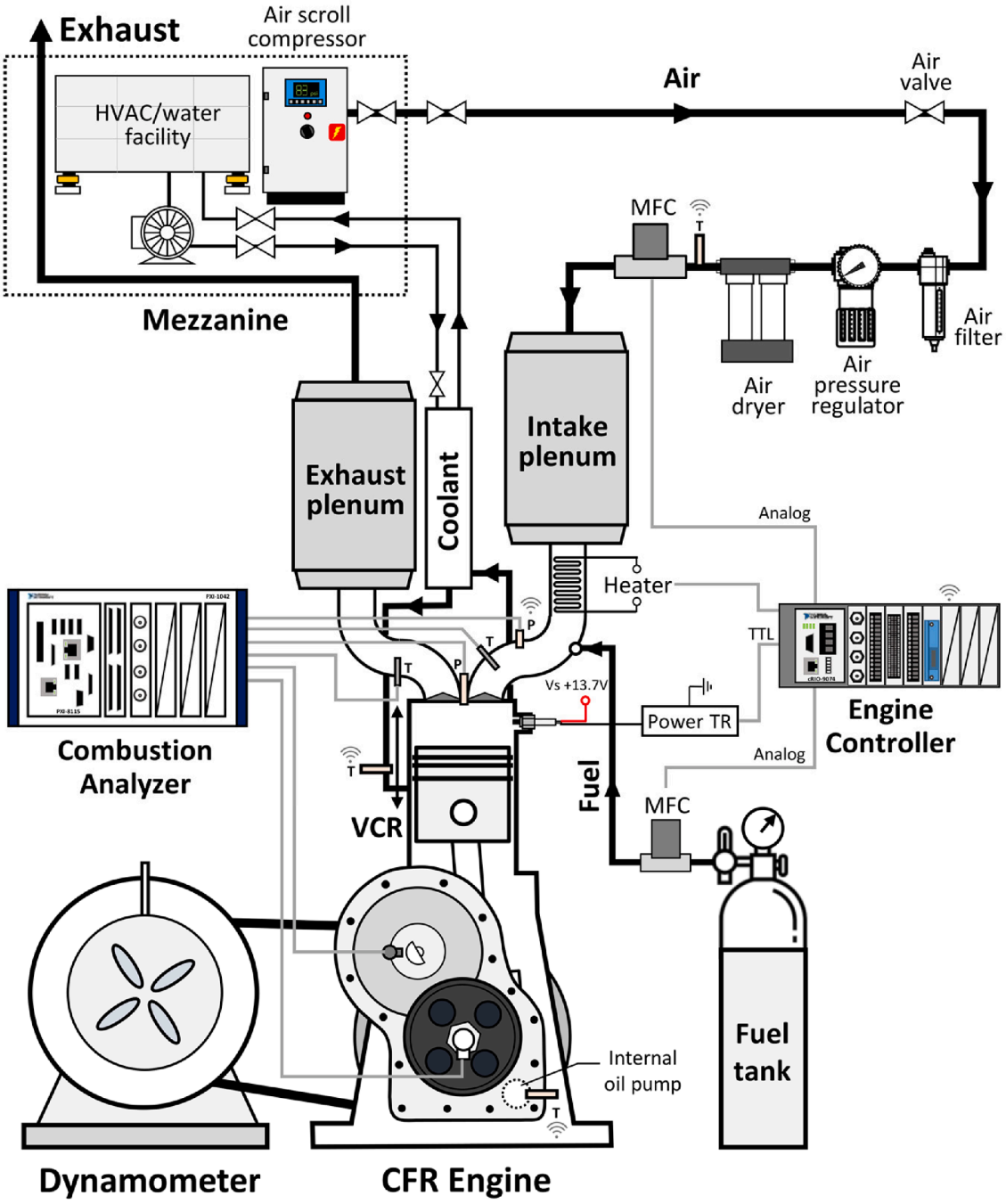

Fig. 3. Configuration of the engine experiment.

Table 2
Engine operating conditions.

Mode	SI mode		CI mode
Load condition	Part-load	Full-load	Wide-open throttle
Compression ratio (-)	9	←	18
Engine speed (rpm)	900	←	←
Intake pressure (bar)	0.865 ± 0.005	1 ± 0.005	←
Spark timing (CA aTDC)	−20	−23	N/A (off)
Equivalence ratio (-)	1	←	var. (<1, lean-burn)
Intake temperature (°C)	200 ± 0.5	←	var.
Coolant temperature (°C)	98.5 ± 0.5	←	←

supply gases, including air, is determined, and it remained unchanged during the experiment while the total flow rate was adjusted to obtain the intake pressure shown in Table 2.

Two main constraints were employed for determining the feasible operating conditions in this study: CoV (covariance) of the gross indicated mean effective pressure (gIMEP) was used to determine the combustion instability. Ringing intensity (RI) was used to quantify the noise level of knocking combustion due to the considerable amount of autoignition and deflagration.

RI was first proposed by Eng [69] to quantify the noise level of an HCCI engine and has been used in many studies to characterize the range of allowable operating noise level. The equation for RI is as follows:

$$RI \cong \frac{1}{2\gamma}\frac{\left(\beta \bullet \frac{dP}{dt}\Big|_{max}\right)^2}{P_{max}}\sqrt{\gamma R T_{max}}[\mathrm{MW/m^2}] \quad (6)$$

where γ is the specific heat ratio of unburned gas at MFB10 (mass fraction burned 10%) burn point, and R is the gas constant of the unburned mixture before combustion. While other studies usually apply a 5 MW/m^2 threshold limit [70,71], a 10 MW/m^2 limit was used in this study in consideration of the high knock durability of the CFR engine and poor ignitability of the baseline fuel. For simplicity, the maximum temperature was computed assuming the residual gas fraction was zero. During the experiments, a fast calculation was required to successfully monitor combustion status; therefore, γ was derived by linear fitting on the log-scaled pressure-volume curve. The discrepancy between the initial simple calculation and detailed calculation thereafter was <5% throughout the experimental campaign.

The CoV of the IMEP in Eq. (7) was used to determine the combustion instability. Gross IMEP (gIMEP) was used in the calculation to solely focus on the combustion event while neglecting the breathing process. During engine testing, moving-averaged value using 300 consecutive cycles was monitored, and the values presented in this study are the averages of two thousand cycles. A 5% limit was applied in this study.

$$CoVofIMEP = \frac{std.dev(gIMEP)}{average(gIMEP)} \times 100[\%] \quad (7)$$

The CI mode experiment in this study extensively focused on realizing self-sustaining operation. Low-carbon gaseous fuels like methane and ethane are resistant to autoignition and have a lower energy density per volume than conventional market liquid fuels. Combustion becomes highly unstable with such fuels due to insufficient thermal loading in the combustion chamber walls during engine operation, leading to poor heat transfer to the intake charge from the walls [72].

Fig. 4 compares non-self-sustaining combustion (upper figure) and self-sustaining combustion (lower figure). In each figure, from the back to the front, cyclic in-cylinder pressure is plotted for every 40 cycles among 2,000 consecutive cycles data, giving plots for 50 cycles. Fig. 4(a) shows the results for pure methane combustion at ϕ (equivalence ratio) = 0.554 and intake temperature of 200 °C, whereas Fig. 4(b) shows the results at a slightly higher equivalence ratio, ϕ = 0.56. It is a subtle difference (0.1 SLPM) in fuel supply, but self-sustaining combustion was achieved at ϕ = 0.56 but not at ϕ = 0.554. The operation with the lower

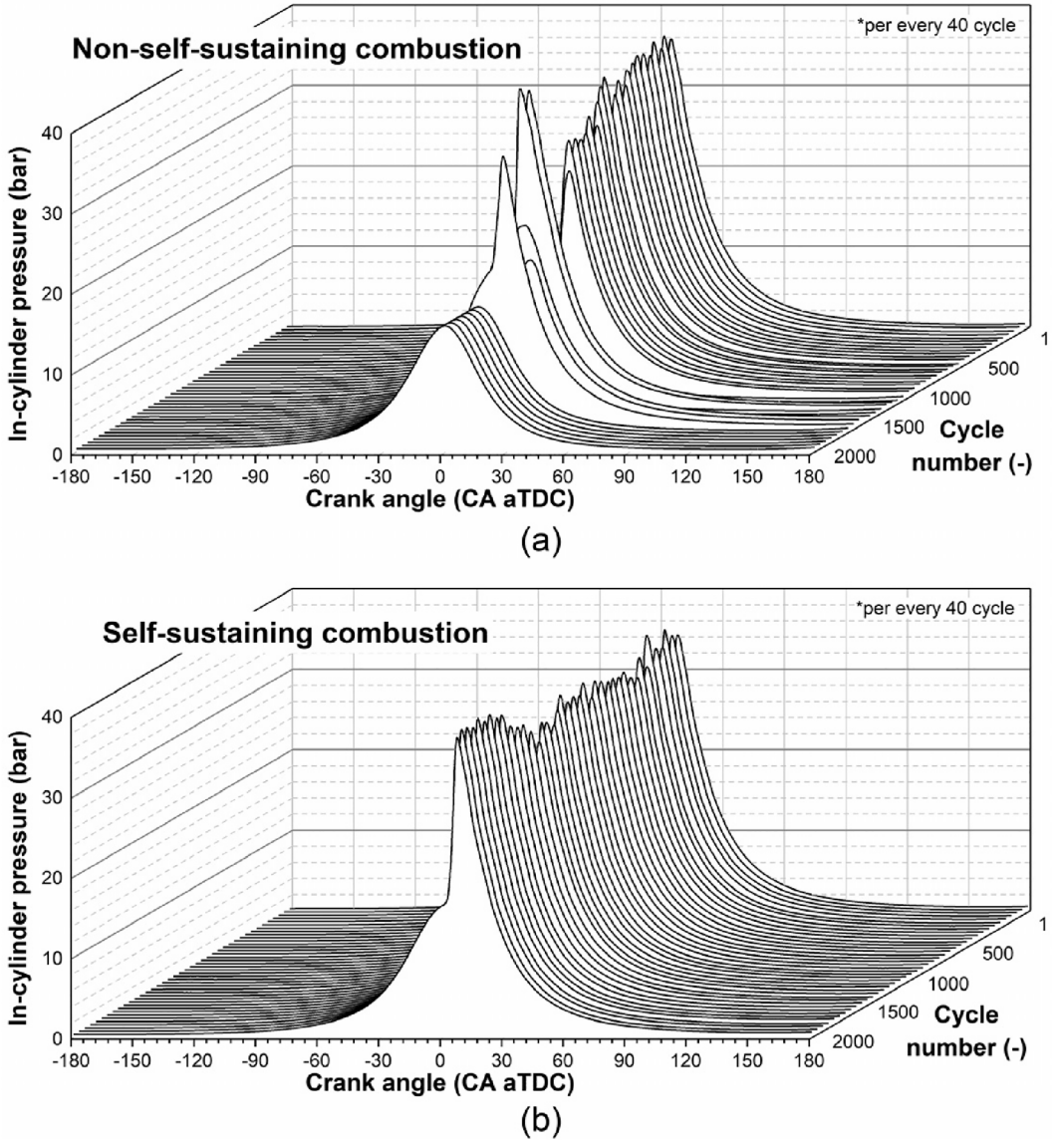

Fig. 4. Example of in-cylinder pressure traces for (a) non-self-sustaining CI and (b) self-sustaining CI. Two thousand consecutive cycles are plotted per every 40 cycles from the back to the front of the figure.

fuel input amount showed a misfire after approximately one thousand cycles. It indicates that repeatable data acquisition could not be carried out by measuring a few hundred cycles, particularly when operating with gaseous fuels. Therefore, fully self-sustaining combustion was maintained for at least two thousand consecutive cycles to achieve a complete steady-state operation. The numbers presented in the paper are ensemble-averaged values of those two thousand cycles, and a very low signal-to-noise ratio was achieved. This experimental methodology and the precise control of flow rates allowed very repeatable results, which was effective for deciding the boundaries of different combustion regimes.

Daily deviation of experiment existed, but it was confirmed that <2% during 3–5 times of repeated experiments of major cases. Averaged RI and CA50 (crank angle at 50% mass burn point) showed the larger daily uncertainties near 5% due to the large cyclic variability and stochastic behavior of knocking combustion, regardless of the adequacy of the unit in CA aTDC.

The fuel and air mixture amount was adjusted to meet the target intake pressure with precise control of the charge temperature. Additional air was induced to the engine to meet the target equivalence ratio on-demand. If the OCM reactor were integrated into the engine, deviations in reactor performance might call for a different air-fuel control strategy. Further study regarding size optimization, design, and control of a reliable OCM reactor is necessary.

As OCM reaction is exothermic, there is an inherent chemical energy loss in the form of heat release. Since the focus of the study is the investigation of the combustion characteristics of fuel modified by OCM, the efficiency was calculated using the LHV of the inlet methane to take such loss into account. The equation for gross indicated thermal efficiency (gITE) is as follows:

$$gITE_{system} = \frac{grosswork}{m_f \times LHV_{CH_4}} \times 100[\%] \tag{8}$$

where m_f is the fuel input mass to the reactor, LHV is the lower heating value of the input fuel (methane, 50 MJ/kg), and the gross work is calculated integrating PdV work over compression and expansion strokes. As this calculation includes the reactor heat loss, a fair evaluation of the OCM reactor application can be made.

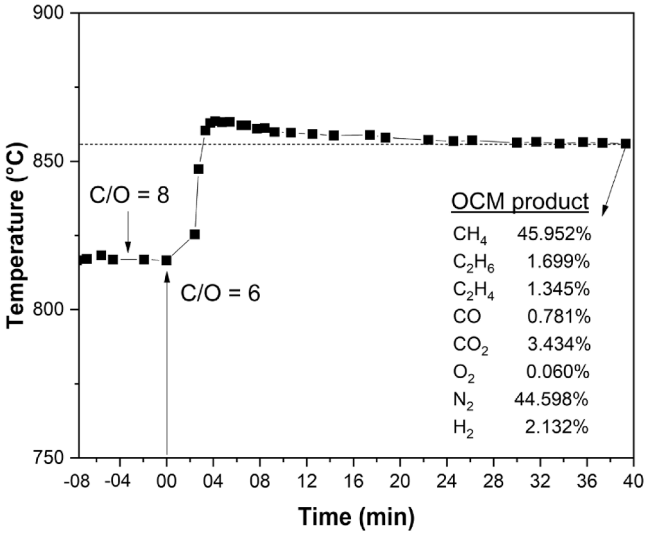

Fig. 5. Temperature change and product composition of OCM reaction benchtop reactor. C/O ratio was changed from 8 to 6 at 0 min.

3. Results and discussion

3.1. Benchtop catalyst reactor results

Fig. 5 shows the outlet temperature results for the benchtop experiment and the composition of the effluent gas mixture. As presented in Table 3, OCM operation at C/O = 6 led to higher C_2 yield than the operation at C/O = 8, and thus the product distribution at C/O = 6 was the mixture used for the later modeling and engine experiments. Catalytic performance depends on many parameters including GHSV, C/O ratio, catalyst mass, catalyst composition, and operating temperature. Therefore, it is difficult to make direct comparison to studies reported in the literature when the conditions are not the same. Nevertheless, the C_2 yields of 10.8% at C/O = 6 and 8.5% at C/O = 8 were observed during the benchtop experiment, these fall within the range of C_2 yield shown in previously reported studies with unsupported Sr/La_2O_3 catalyst in fixed bed reactors; for example, Sollier et al. [44] achieved 7.5–9 % C_2 yield at similar stoichiometry, while Choudhary et al. [41] achieved 18–20 %.

As shown in Fig. 5, realistic OCM products consist not only of methane and C_2 species, but also nitrogen, hydrogen, and carbon oxides. A significant portion of the product stream consists of nitrogen because the air was used as the oxidizer. In the experiments reported here, the reactant stream was also diluted with 10% nitrogen to moderate the extreme heat release and limit catalyst hotspots known to deactivate OCM catalysts. When using OCM products as an engine fuel, gas mixture dilution with nitrogen may affect combustion characteristics and lead to results that are not reflective of combustion characteristics without diluent. However, combustion will be improved without the dilution effect, especially in terms of IDT, so the effect of additional N2 was neglected in this study. The addition of hydrogen to a methane-air mixture has been found to increase the reactivity of the gas mixture, laminar flame speed, and flame stability [73,74]. Thus, the presence of hydrogen in the OCM product stream may result in a favorable change in combustion characteristics of the modified fuel. Therefore, the presence of excess diluent and hydrogen is important when using OCM products as fuel.

To evaluate the combustion properties of OCM products at a deeper level, six different gas mixtures were derived from the OCM catalyst experiments. The molar compositions considered are shown in Table 4. Fuel A was 100% methane fuel, and fuel F was the OCM composite product from the benchtop experiment at C/O = 6. Fuel F was prepared without nitrogen so that nitrogen could be added later to investigate its dilution effect on combustion. Fuels B to E were derived to examine the effect of each fuel's components on engine combustion. For example, fuel B was prepared to observe the effect of C_2 species on shortening the ignition delay when compared to pure methane (fuel A). Fuel C was used to investigate the effect of nitrogen addition when compared to fuel B. Fuel D was prepared to observe the effect of additional CO_2. Fuel E was prepared without hydrogen to compare its combustion characteristics against those of fuel F, which contained hydrogen.

Due to the limited number of flammable gas cylinders allowed in the laboratory, simultaneous feeds of ethane and ethylene from independent sources were not possible. Thus, only ethane was used to investigate the effect of additional C_2 species experimentally. Its concentration was set to the sum of ethane and ethylene concentrations from the benchtop experiment. The original gas compositions with both ethane and ethylene were used for the computational investigation; the numbers in parentheses in the fuel B column indicate the concentrations used for the computation.

Table 3
Benchtop catalyst performance at C/O = 6 and 8.

C/O	Methane conversion	C_2 selectivity	C_2 yield
6	18.2	59.5	10.8
8	16.5	52.8	8.5

Table 4
Fuel mixture compositions used in the engine experiments [%vol].

Fuel	A	B	C	D	E	F
Specification	Methane	A + C_2	B + N_2	C + CO_2	F – H_2	OCM
CH_4	100	93.8	49.1	47.4	47.0	46.0
C_2H_6	–	6.2 (3.5)	3.3	3.1	1.7	1.7
C_2H_4	–	(2.7)	–	–	1.4	1.35
CO	–	–	–	–	0.8	0.78
CO_2	–	–	–	3.5	3.5	3.4
O_2	–	–	–	–	0.06	0.06
N_2	–	–	47.6	46.0	54.46	44.58
H_2	–	–	–	–	–	2.13
Sum	100	100	100	100	100	100

3.2. Fuel combustion characteristics

3.2.1. Laminar flame speed

Fig. 6 shows the laminar flame speed (LFS) at 1 bar and 298 K for fuel A (100% methane), fuel B (methane with C2 species), and fuel F (OCM product), calculated with different mechanisms and at various equivalence ratios. The three mechanisms were extensively validated at this condition, thus the LFS results exhibit very similar trends. That is, the addition of C_2 species increases the LFS regardless of the equivalence ratio. Fuel F shows the lowest LFS although it has C_2 species. This is likely due to the presence of inert gases such as CO_2 and N_2.

In real world conditions, the in-cylinder condition undergoes extreme pressure and temperature changes. Experimental validation of LFS at these high temperature-pressure conditions has not been well established [54]. A shock tube experiment is a viable solution for experimental measurement of the LFS, and Ferris et al. [75] reported that various mechanisms, including GRI 3.0 and Aramco 3.0, showed agreeable validation results under high-temperature conditions.

Fig. 7 shows the calculated LFS with the Aramco 3.0 mechanism for the same fuels A, B, and F at 20 bar and 900 K. This condition was chosen to roughly replicate the in-cylinder condition at the top dead center (TDC) at compression ratio 9, therefore it is expected that the calculated LFS would be similar to that of the unburned gas in the combustion chamber during SI combustion. In general, pressure elevation increases the activation energy of reactions, so an increase in termination reaction rates is faster than that of branching reactions, resulting in an overall decrease in LFS [76]. However, the overall LFS was significantly increased compared to the previous standard condition of 1 bar and 298 K. This increase is attributed to the increase in temperature caused by the pressure increase through the polytropic process. The same trend as the standard condition (Fig. 6) is shown at this condition: the addition of C_2 species enhances the LFS (in fuel B), but the presence of other species (in fuel F) leads to slower LFS, even slower than the LFS of pure methane (fuel A).

As shown in Fig. 5 and Table 4, N2 and CO_2 account for the majority of OCM products. Such inert gases have three major effects [77] on LFS: dilution, thermal diffusion (heat capacity [78]), and chemical. The dilution effect decreases LFS due to the presence of diluent in the

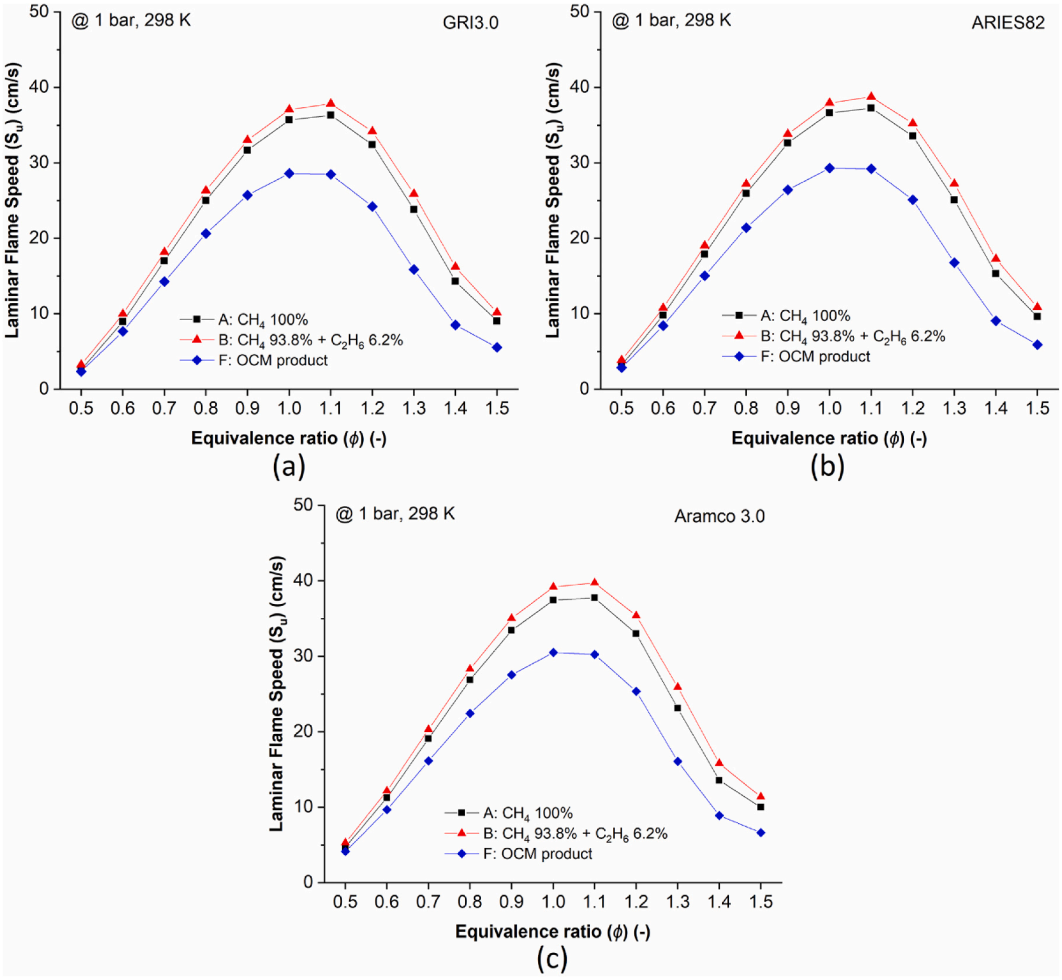

Fig. 6. Laminar flame speed of the fuels with different mechanisms at 1 bar and 298 K; (a) GRI3.0; (b) ARIES82; (c) Aramco 3.0. Fuels are methane (fuel A, black line with square), C_2 added fuel (fuel B, red line with triangle), and OCM product (fuel F, blue line with diamond). Fuel B contains 3.5% of ethane and 2.7% of ethylene. (For interpretation of the references to color in this figure legend, the reader is referred to the web version of this article.)

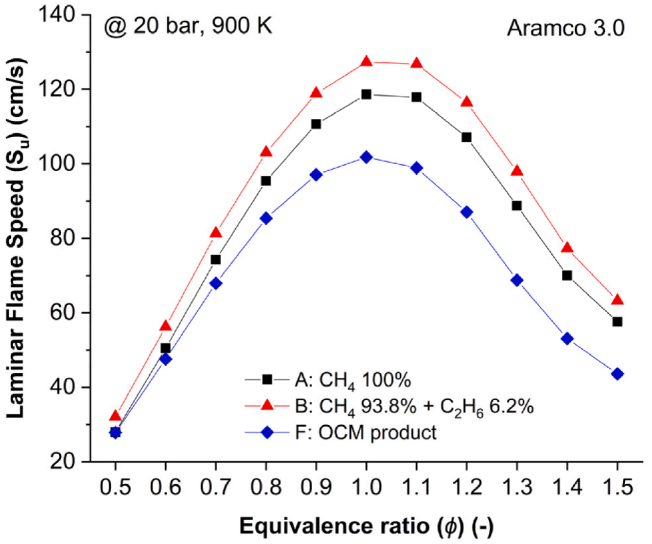

Fig. 7. Laminar flame speed of the fuels A, B, and F with Aramco 3.0 mechanism at 20 bar and 900 K.

reactant. The thermal diffusion effect is the impact of diluent to the specific heat capacity of a gas mixture which leads to the overall change in the temperature profile during thermodynamic process. The chemical effect is the change in chemical kinetics due to the presence of diluent. A recent study [77] reported that dilution is dominant over the other effects in a premixed methane/air environment. Their finding accords with LFS calculation results shown in Figs. 6 and 7, where fuel F consists largely of diluents and has the slowest LFS.

Combustion duration is a critical factor in determining thermal efficiency; faster combustion allows a cycle to more closely follow the ideal Otto cycle and is beneficial for knock resistance. However, the slower LFS of the modified fuel is disadvantageous for SI combustion as it can lead to slower combustion than pure methane combustion.

3.2.2. Ignition delay time

Fig. 8 illustrates the IDT of fuels A and F. The white line represents the pressure-temperature (P-T) trajectory (2.5 crank angle interval) of engine operation at compression ratio 18 and wide-open throttle (WOT). It is plotted as a reference to visualize the benefit of fuel modification during actual engine operation. The black cross marks the start of combustion. Fuel A exhibits poor auto-ignitability indicated by the long IDT shown in Fig. 8(a), making it unsuitable for CI combustion. The mixture cannot combust at a low compression ratio due to the long IDT unless it is heated unrealistically high before the compression process. Fig. 8(b) shows decreased IDT of fuel F compared to fuel A. The decrease is mainly attributed to the shorter IDT of C_2 species and corresponds roughly to a 25 K increase in initial mixture temperature.

The reference engine trajectory passes the region where the IDT is more sensitive to change in temperature than pressure. The IDT significantly decreases as the engine trajectory approaches TDC. Due to the polytropic relation between pressure and temperature, the slope of the P-T trajectory becomes steeper. Therefore, it appears that the advantage of further increasing the compression ratio would be somewhat limited. Instead, it can be suggested that heating the gas mixture before induction is effective for promoting the combustion.

The contour plots for merit in IDT (mIDT) as defined in Eq. (5) are illustrated in Fig. 9. The red color indicates higher mIDT (shorter IDT), and blue indicates little or no advantage. Fig. 9(a) shows the mIDT of fuel B, which contains C_2 additives in addition to pure methane, and Fig. 9(b) shows fuel F's mIDT. As can be seen, both fuels B and F show shorter IDT than pure methane (fuel A), i.e., larger mIDT than unity. Only a subtle change is found between the two fuels, indicating that the

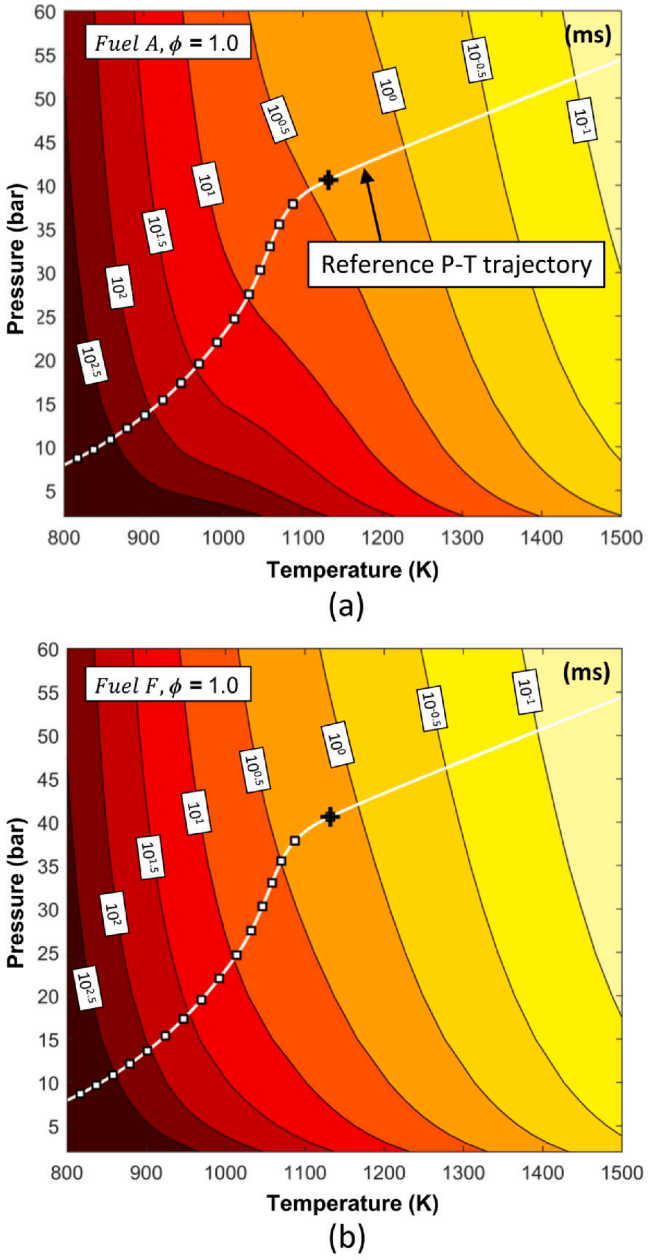

Fig. 8. IDT at $\phi = 1.0$ in the pressure–temperature domain; (a) Fuel A; and (b) Fuel F. The white line shows a reference P-T trajectory of CI combustion at compression ratio 18. Isolines of the contour are drawn in log-scale.

presence of inert gases in fuel F did not significantly increase the IDT from that of fuel A, and the advantage to the IDT by C_2 species remains relatively the same in both fuels.

mIDT varies across the pressure and temperature range. Although the change is subtle, mIDT is lower for fuel F than for fuel B in the lower temperature region where the P-T trajectory of the early compression stage lies. A larger decrease in IDT comes from when using OCM fuel. mIDT is higher for fuel F at temperatures beyond 1100 K, but this temperature region is not reachable during engine operation. Because the heat capacities of fuels B and F were almost identical, it is believed that the further decrease in the IDT for fuel F originates from the chemical effect of other gas components such as CO and H_2.

No known previous study has comprehensively analyzed the individual effect of CO and H_2 on the IDT of methane-based fuel under engine-relevant conditions. However, Subramanian et al. [79] investigated those effects for n-heptane combustion and found that a very small

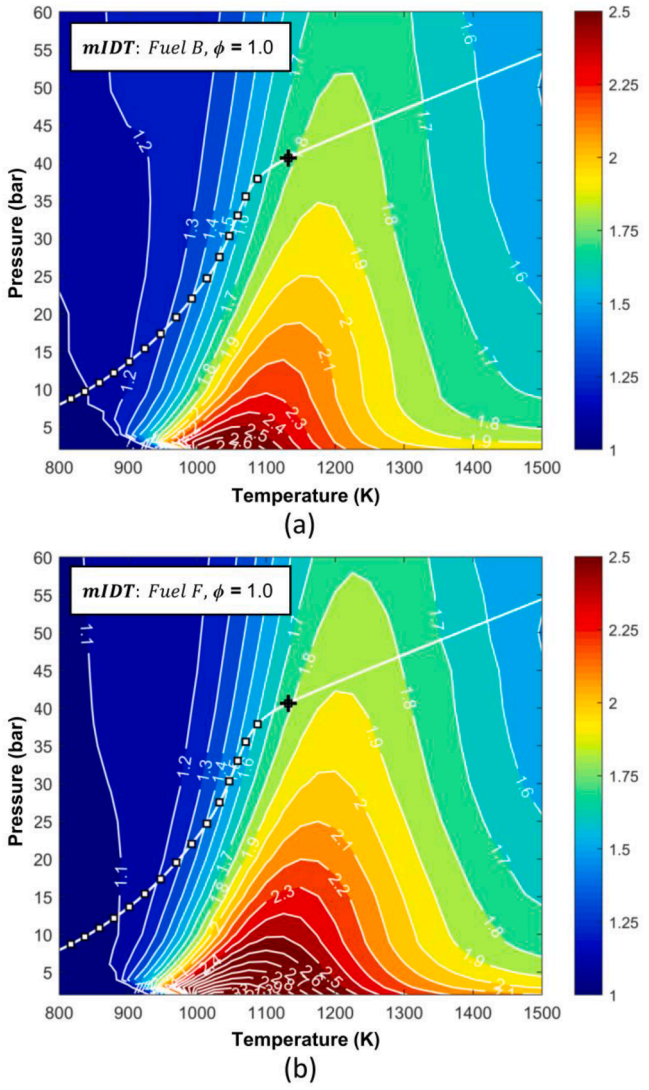

Fig. 9. mIDT at $\phi = 1.0$ in pressure–temperature domain; (a) Fuel B; and (b) Fuel F.

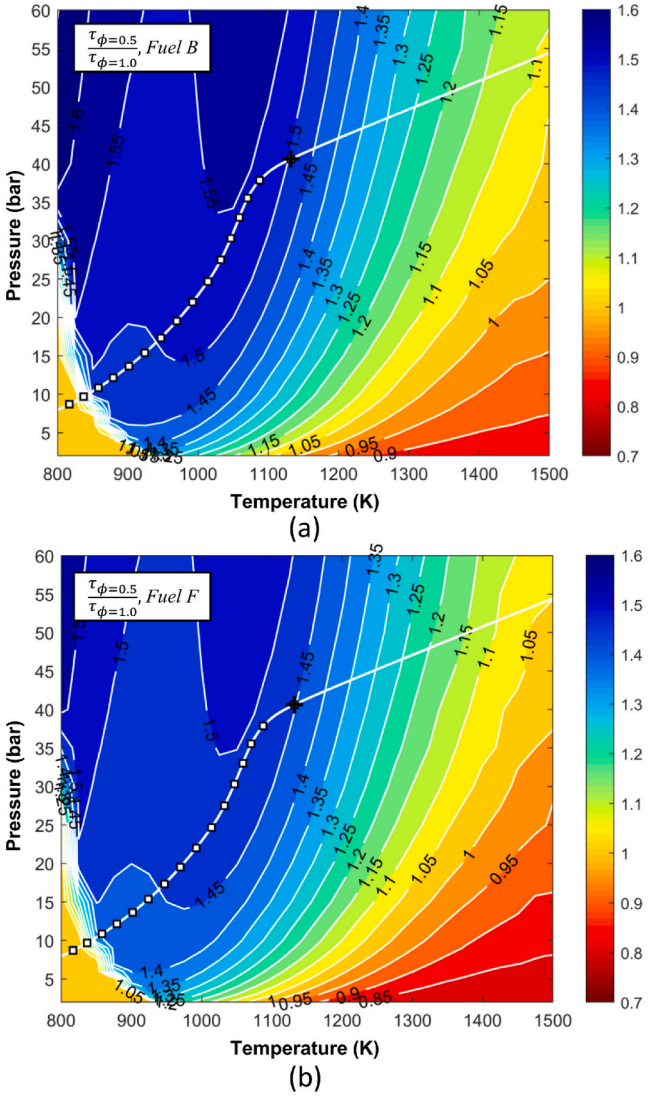

Fig. 10. Ratio of IDTs for $\phi = 0.5$ to $\phi = 1.0$ in pressure–temperature domain; (a) Fuel B; and (b) Fuel F.

amount of CO decreased IDT at high temperature (1000 K) but increased IDT at a low temperature (600 K). It was also found that H_2 delayed ignition at low-temperature but did not substantially affect IDT in a high-temperature environment. A more fundamental study incorporating sensitivity analysis is required to investigate this phenomenon. Nonetheless, the results from this study also illustrate that operating OCM fuel at high temperatures is beneficial for decreasing IDT due to the presence of both C_2 species and CO.

The isolines near the engine trajectory in Fig. 9 have a very similar slope to the P-T trajectory, particularly at the end of the compression stroke. This indicates that increasing compression ratio does not have a substantial benefit on IDT, in a similar manner to Fig. 8. In practice, it is recommended to apply techniques that efficiently increase the initial mixture temperature, like thermodynamic recuperation with optimized reactor design or employing a turbocharger to recover waste heat and/or to increase intake mixture temperature by boosting.

Fig. 10(a and b) show the IDT ratios of lean-burn condition to stoichiometric condition, $\tau_{\phi=0.5}/\tau_{\phi=1}$, for fuels B and F, respectively. The lower values (close to red color) indicate shortened IDT, and the higher values (close to blue) indicate prolonged IDT compared to stoichiometric conditions. The figures show that the IDT ratio is greater than unity for both fuels at relevant conditions. However, the IDT ratio was lower (IDT was less prolonged) for fuel F than for fuel B. This is attributed to the presence of CO in fuel F, which acts as an autoignition enhancer, especially for leaner mixtures at high temperatures [79]. In addition, it has been reported that IDT being prolonged by hydrogen addition can be suppressed in lean-burn conditions. Because of that, with the presence of both CO and H_2, the disadvantage on IDT by dilution becomes less significant in fuel F. Although the change is not noteworthy between the two fuels, it demonstrates that the effect of OCM products on IDT is at least equivalent to that of C_2-added fuel despite the presence of inert gases. For CI combustion, leaner combustion has several advantages over stoichiometric conditions that are more compatible with OCM fuel characteristics: less pumping work by wide-open throttling or boosting, less pressure rise rate to lower the noise level, and enhanced thermal efficiency by increased specific heat ratio.

Earlier in the study, it was concluded that the modified fuel, fuel F, exhibits decreased LFS, which adversely affects SI mode combustion at a low compression ratio. Here, the mIDT results show that fuel F can be advantageous when operating under lean-burn condition at a relatively high compression ratio, i.e., CI mode, due to the reduction in IDT compared to 100% methane (fuel A). Furthermore, although not presented in this paper for brevity, the same computations carried out using the GRI 3.0 and ARIES82 mechanisms showed the same conclusions as Aramco 3.0 mechanism.

3.3. Engine combustion characteristics

3.3.1. Spark-ignition mode experiment

Fig. 11 illustrates the results at the part-load condition of spark-ignition mode: in-cylinder pressure (a) and heat release rate (HRR) (b) against crank angle. The markers are at a 1.5 CA interval, and CA50, the combustion phasing, is also indicated with the HRR. Maximum brake torque (MBT) was identified (20 CA bTDC) with a set of spark timing sweep experiments using fuel A (gIMEP 5.26 bar). Fuel was changed while maintaining other parameters were kept consistent (see Table. 2 for details). The RI was very low for all operating points (<0.5 MW/m^2).

The CFR engine was originally designed to study engine knock, so the spark plug is located in a lateral position, indented at the top of the cylinder side wall. This design is less advantageous for initial flame propagation than a typical vertical central-mount type, resulting in a slow increase in HRR in the initial stage, as shown in Fig. 11. The figure also shows that combustion phasing was advanced by adding C_2 species (fuel B): CA50 decreased from 6.8 to 4.3 CA after top dead center (aTDC). The flame propagated faster throughout the cycle, which aligns well with the LFS simulation result. When the fuel was changed from A to B, gITE increased from 29.95% to 30.44%, and gross indicated specific fuel consumption (gISFC) decreased from 240.26 g/kWh to 236.42 g/kWh. However, it is apparent that the increase in gITE would have been more significant if the spark timing had been optimized for the changed fuel.

Retardation of the combustion phasing was found for fuel F, the OCM product fuel. CA50 was retarded to 10.8 CA aTDC, which was also suggested by the LFS result. The reduced LFS by the addition of other inert gases led to a longer combustion duration. The turbulence in the CFR engine is weaker than in typical production engines due to a lower tumble motion, and this characteristic increases the dominance of LFS to combustion duration. For fuel F, gISFC increased to 253.60 g/kWh (gITE = 28.38%), and is 5.6% detrimental when compared to baseline.

Fuel E was introduced to evaluate the impact of the absence of hydrogen in the OCM product. Concentrations of other components were the same as fuel F except without hydrogen. Hydrogen is a well-known LFS enhancer when added to low-carbon gaseous fuels [80]. However, as seen in the figure, only a very subtle change (advancement) of the combustion phasing (CA50 from 11.8 to 10.8 CA aTDC) was observed over fuel E (w/o hydrogen). The effect was limited due to its low mass fraction in the fuel mixture. While hydrogen accounts for a 2% volume fraction in fuel F, it is only 0.19% of the mass fraction of the fuel and 0.021% of the total air and fuel mixture.

Fig. 12(a and b) present the results at the full-load condition for fuels A and F. For fuel A, 6.0 bar of gIMEP was the highest load due to the low

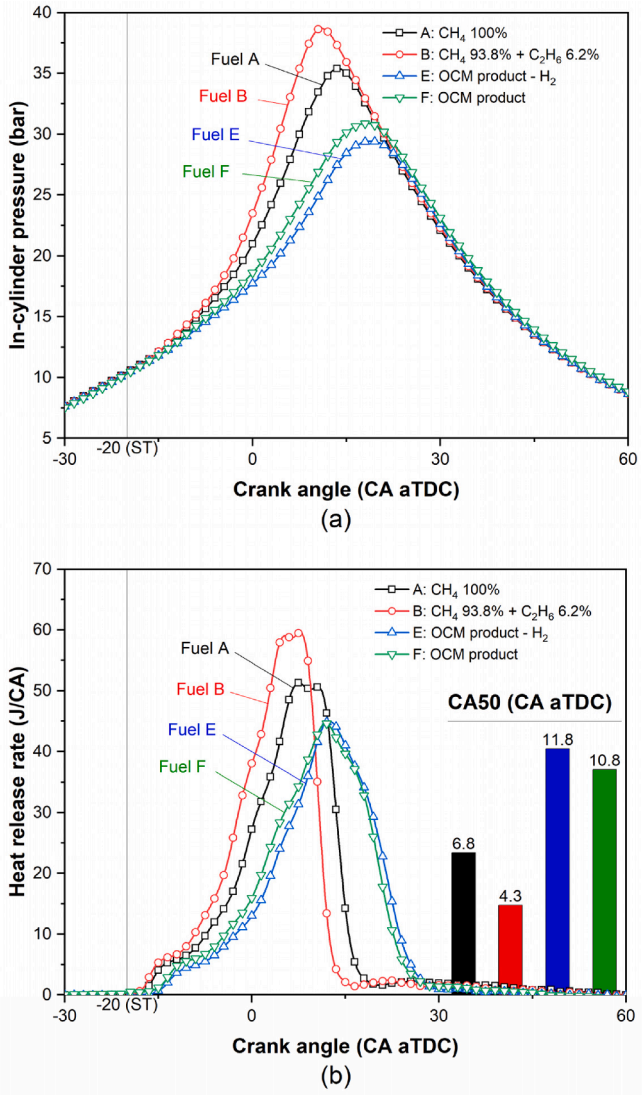

Fig. 11. Results at the part-load condition in spark-ignition mode using fuels A, B, E, and F: (a) In-cylinder pressure; and (b) Heat release rate.

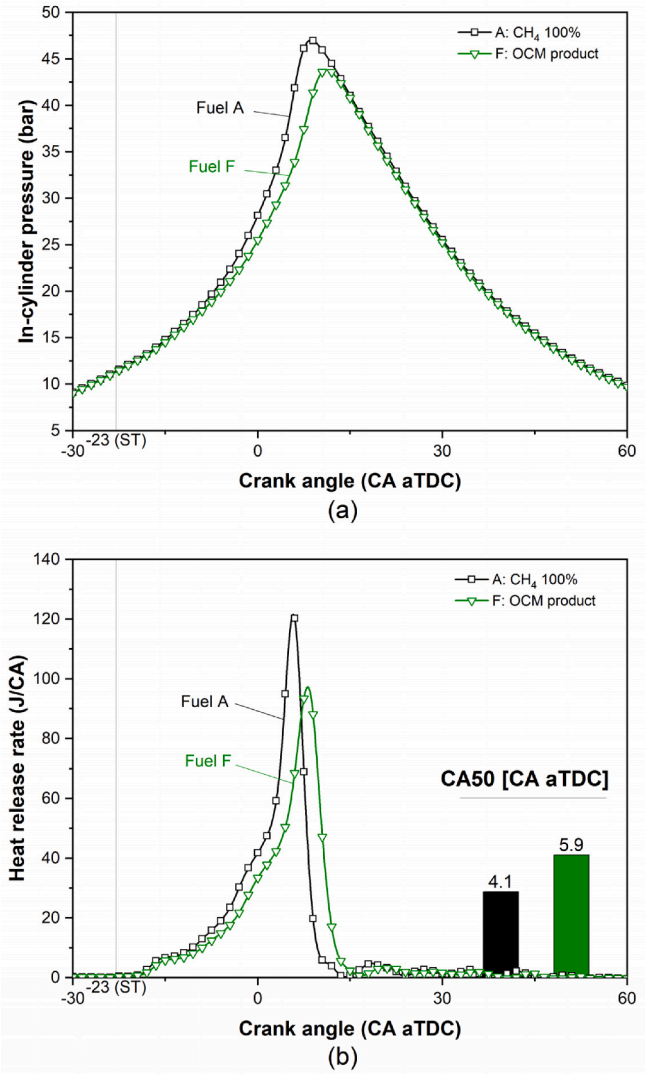

Fig. 12. Results at the full-load condition in spark-ignition mode with fuels A and F: (a) In-cylinder pressure; and (b) Heat release rate.

volumetric efficiency of port-induced gaseous fuel. MBT spark timing was 23 CA bTDC as indicated in the figures, and CA50 was 4.1 CA aTDC. The RI was higher (2.31 MW/m^2) than under the part-load condition. The temperature increase followed by the pressure (load) increase led to faster combustion than in the part-load condition, and the burn duration (CA10–90) decreased from 18.0 CA to 15.3 CA. When fuel A was replaced by fuel F, combustion was prolonged as in the part-load condition. CA50 was retarded from 4.1 to 5.9 CA aTDC despite identical spark timing (23 CA aTDC), thereby decreasing the load to 5.88 bar of gIMEP. gITE also decreased by 4.5%, from 31.74 to 30.31%.

In summary, the addition of C_2 species to methane reduces combustion duration in spark-ignition mode due to their higher LFS. However, this advantage is overshadowed by the dilution effects of other species found in OCM products like CO_2 and N_2. Combustion with the OCM products resulted in a net increase in combustion duration compared to methane alone. Based on the LFS simulation results, lean-burn conditions would be expected to show a similar result; OCM product fuel is not suitable for SI combustion.

3.3.2. *Compression-ignition mode experiment*

CI experiments were conducted using premixed gaseous fuel input. In this combustion mode, flame propagation is suppressed in favor of a faster compression-induced combustion process. After the intake valve is closed, the gas mixture in the closed cylinder is compressed by the piston's upward movement, reducing the IDT of the mixture as the temperature and pressure increase. When the thermodynamic state reaches the ignition point, ignition occurs in a distributed manner but relatively fast throughout the combustion chamber. CI combustion with a considerable amount of spontaneous autoignition (equivalent to HCCI) is generally thought to have high thermal efficiency due to its short combustion time, like constant volume combustion, i.e., ideal Otto-cycle. However, combustion cannot occur spontaneously across the chamber; instead, it occurs in a finite time scale. Therefore, overly advanced combustion phasing may lead to an undesirable loss of useful work due to increase in negative compression work. It is also challenging to control the combustion phasing because of the long and temperature-dependent IDT of methane fuel; consequently, it is very likely that combustion occurs near the top dead center, provoking large negative compression work and large heat transfer loss. Therefore, retarding combustion phasing by controlling IDT is pivotal in increasing CI combustion efficiency while maintaining combustion stability.

Fig. 13 shows the results of pure methane (fuel A) combustion in the engine. Methane has considerably long IDT and poor auto-ignitability, so operation is not practically feasible without a considerable increase in intake temperature [18]. Fig. 13(a) shows several in-cylinder pressure curves. The black dashed line with open circle indicates the case at intake temperature of 200 °C and equivalence ratio of 0.55. The operation was not feasible under this condition. Unlike other cases, the curve at $\phi = 0.55$ was plotted using only five-cycle average data after a complete misfire, because the MFC decreased the pressure to maintain the flow rate caused by decrease in wall temperatures after the misfire.

By contrast, the curve representing equivalence ratio 0.56 (dotted line with rectangle marker) displays successful and self-sustaining CI. This equivalence ratio corresponds to the minimum equivalence ratio at $T_{in} = 200$ °C in Fig. 13(b), and the equivalence ratio of self-sustaining operation as previously described. The solid line with triangle markers in Fig. 13(a) is at a lower charge temperature (160 °C), and more fuel is required to achieve stable combustion ($\phi = 0.613$).

The start of combustion was kept similar, and CA10 was within 2 ± 0.5 CA aTDC for all pure methane combustion cases. Although the IDT of methane is predominantly affected by the change in temperature, the impact of the equivalence ratio is not negligible. More fuel leads to higher thermal loading of the chamber walls, so this compensation led to very similar autoignition timings.

Fig. 13(b) shows the RI, gIMEP, and minimum equivalence ratio to enable combustion using fuel A as a function of intake charge temperature. From right to left, the charge temperature was decreased from 200 °C to 160 °C. More fuel, i.e., a higher equivalence ratio, was required to produce enough thermal loading to achieve combustion when the charge temperature was decreased. Even though self-sustainability was achieved, pure methane operation is not practically feasible due to significantly high RI (>10 MW/m^2), and RI increased continuously up to 16 MW/m^2 at $T_{in} = 160$ °C as the input fuel amount increased. Anecdotally, the engine noise was also very loud in these conditions.

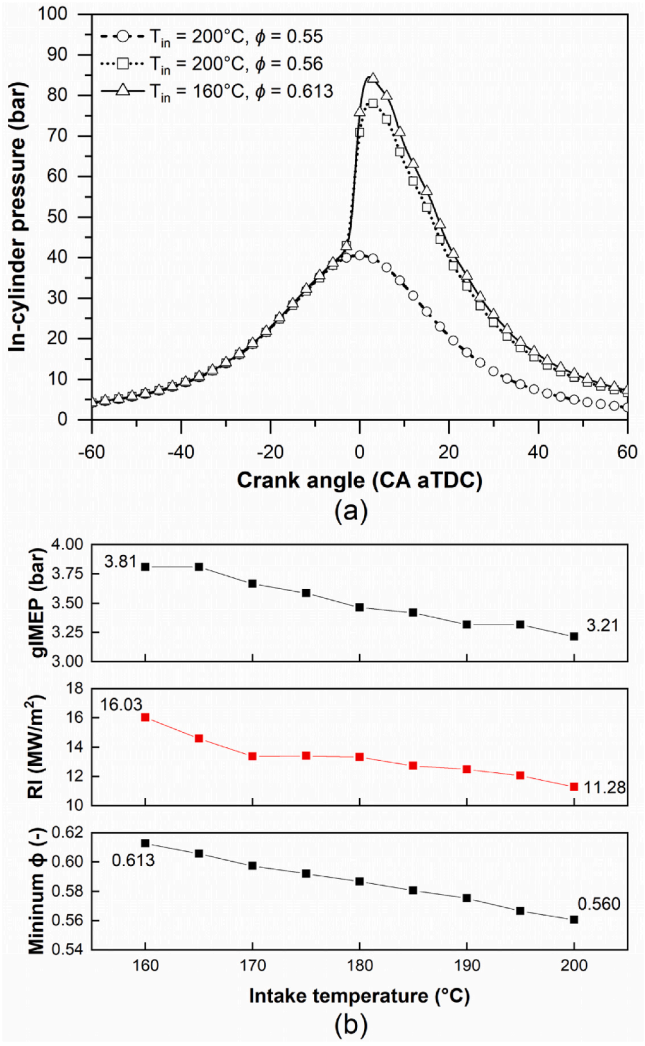

Fig. 13. Experimental results of CI combustion using fuel A (pure methane): (a) In-cylinder pressure; and (b) Experimental outputs against intake charge temperature.

Fig. 14 shows (a) in-cylinder pressure and (b) HRR of the five fuels tested. While the supplied fuel was changed, the equivalence ratio and intake charge temperature were maintained at 0.56 and 200 °C, respectively. Fuel A, the pure methane baseline fuel, corresponds to the data point of the 200 °C case in Fig. 13(b). As can be seen, fuel B exhibits a remarkable advancement of combustion phasing. This confirms that the addition of C_2 species significantly decreases IDT. By contrast, fuel C, the addition of nitrogen to fuel B, resulted in retarded combustion phasing compared to fuel B. This is attributed to the prolonged IDT from the dilution effect of nitrogen [81].

The addition of CO_2 (fuel D) showed further retardation from fuel C by increasing IDT in the same manner. This result contradicts Langille et al. [45], who showed no substantial change by CO_2 addition using an opposed flow reactor experiment. While it is not clear why such a small

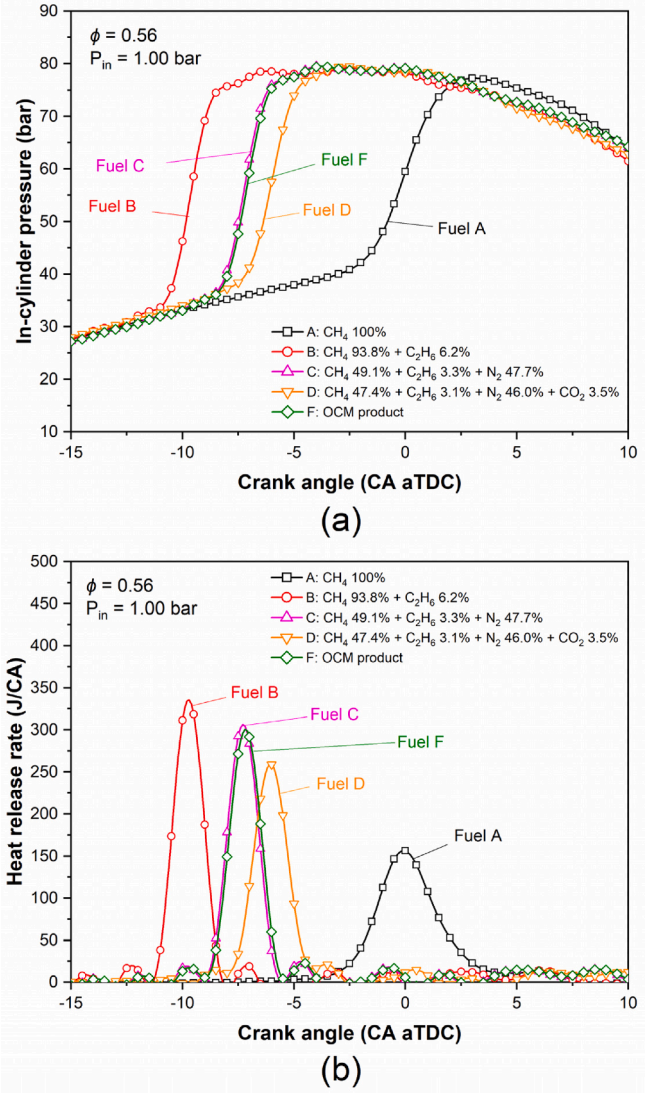

Fig. 14. Engine experimental results of CI combustion with fuel change: fuels A–D and F at $\phi = 0.56$, $T_{in} = 200$ °C and $P_{in} = 1$ bar: (a) In-cylinder pressure; and (b) Heat release rate.

amount of CO_2 results in substantial change, it is known that increased dilution leads to longer IDT. Furthermore, N_2 and CO_2 are the main contributors to increase IDT when using exhaust gas recirculation in conventional engines. In previous work, increased thermal diffusion (heat capacity) effect was reported as the largest contributor of longer IDT [71], while the dilution effect was the primary source of LFS decrease. Further investigation on the effect of diluents on IDT may be needed to elucidate the phenomenon. Nevertheless, fuel D shows significantly advanced combustion phasing compared to the baseline. Therefore, contrary to the findings for SI combustion mode, the advantage of C_2 addition in CI combustion outweighs the disadvantage from diluents.

When OCM product (fuel F) was supplied, a slight advancement in combustion phasing was again observed. Other constituents such as hydrogen and ethylene decreased the IDT; Unlike fuels B-D, fuel F contained ethylene as part of its C_2 products, as explained earlier. Hydrogen is also known as an IDT reducer [19,75,76], whereas CO increases IDT [82]. The result here indicates that the advantage from H_2 and C_2H_4 was more influential than the disadvantage of having CO.

The reactivity increase by OCM did not necessarily enhance the system efficiency under the conditions tested. The combustion of the baseline condition occurred near TDC, so the improved reactivity by the fuel modification advanced the combustion phasing and reduced the efficiency due to the increased negative compression work. The OCM product may provide some capability to retard combustion phasing, thereby improving the efficiency. Retardation of the combustion phasing to increase the efficiency could only be enabled by decreasing the equivalence ratio, i.e., reducing the fuel input amount, and cooling the intake charge temperature. However, both strategies increase combustion instability; therefore, it is necessary to balance any efficiency advantage with the risk of combustion instability.

A retardability experimental result using fuel F is shown in Fig. 15, visualizing short combustion durations of the CI mode. The charge temperature (T_{in}) was maintained at 200 °C, and the equivalence ratio was decreased to retard the combustion. The intake pressure was kept at 1 bar throughout the conditions. Self-sustaining operation could not be achieved with fuel A at $\phi = 0.55$ (dashed black line) due to misfires and only shown as the motoring trace in Fig. 15(a). Therefore, the baseline condition was $\phi = 0.56$ with fuel A. At the same equivalence ratio, the combustion was significantly advanced when fuel F was used, and the combustion phasing was retarded as the equivalence ratio decreased to 0.375 with a 0.025 decrement.

Fig. 16 shows the output parameters of the experiment. Each

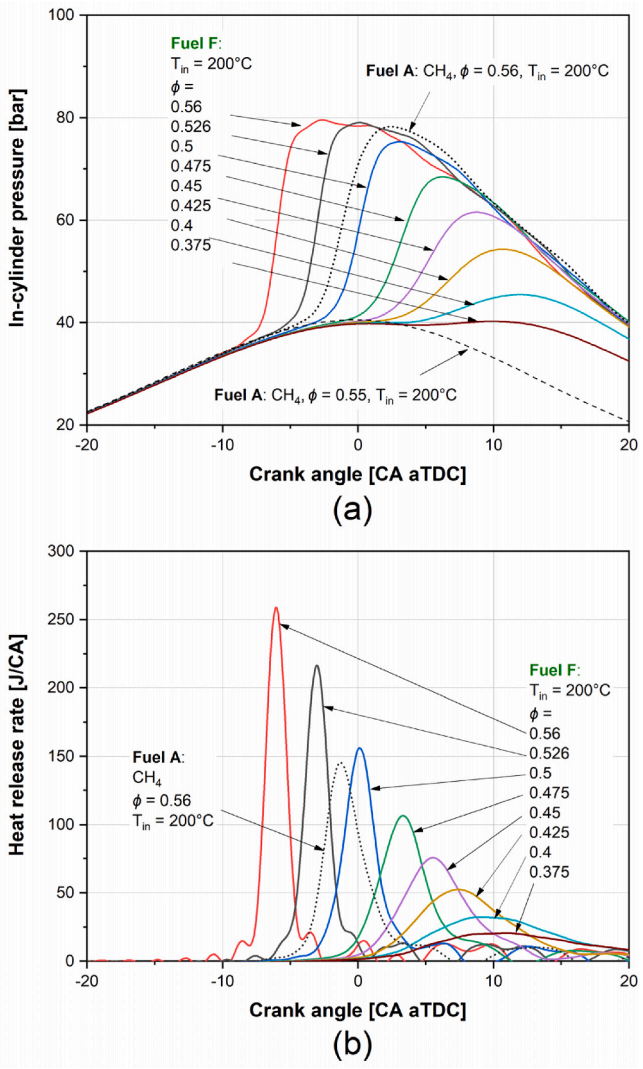

Fig. 15. Engine experimental results for CI combustion the variation in equivalence ratio using fuel F at $T_{in} = 200$ °C and $P_{in} = 1$ bar: (a) In-cylinder pressure; and (b) Heat release rate.

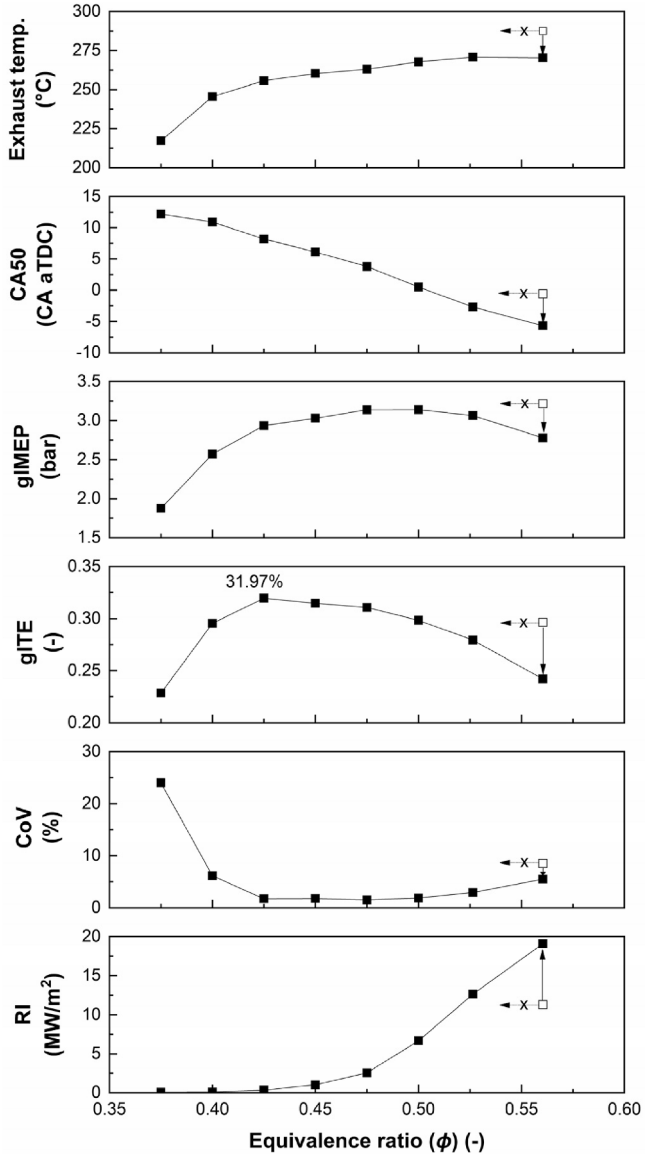

Fig. 16. Engine experimental results for CI combustion with the variation in equivalence ratio using fuel F at T_{in} = 200 °C and P_{in} = 1 bar: output parameters (exhaust temperature, CA50, gIMEP, gITE, CoV of gIMEP, and RI).

parameter is shown against the equivalence ratio. The open squares in the figure represent the values of the baseline case, of which the 'x' mark means that the equivalence ratio could not decrease more due to the poor combustion stability (increase in CoV of IMEP, or misfire). Sold lines with markers indicate fuel F. When the fuel changed from A to F, the load (gIMEP) decreased because of the overly advanced combustion phasing (see CA50), and the efficiency (gITE) decreased accordingly.

Fig. 16 shows the results. The open squares in the figure represent the values of the baseline (fuel A), and the arrows with the 'x' mark mean that the equivalence ratio for fuel A could not be reduced further due to poor combustion stability. The solid lines with markers indicate fuel F. When the fuel changed from A to F, the load (gIMEP) decreased because of the overly advanced combustion phasing (see CA50), and efficiency (gITE) decreased accordingly.

For fuel F, exhaust temperature decreases when the fuel-air ratio decreases (from right to left). The effect of temperature reduction by decreased fuel amount is larger than the increase in exhaust enthalpy from retarded combustion phasing. The load first increases and then decreases after plateauing, where the maximum load is at $\phi = 0.5$. As combustion is retarded, negative compression work and heat loss decrease, and expansion work increases; thus, gIMEP increases despite the reduced fuel amount. When combustion was retarded, the gITE increased from 24.2% at $\phi = 0.56$ to 31.97% at $\phi = 0.425$, and a slight decrease in load was observed below $\phi = 0.5$; the system efficiency was enhanced by 24.3% due to the enhanced reactivity and controllability of the combustion phasing. It can be said controlled autoignition (CAI) was enabled by the OCM fuel pre-treatment.

When the equivalence ratio was decreased, CoV initially decreased, and then increased again at ϕ below 0.475. The decrease of CoV at a higher equivalence ratio does not correspond to an improvement in combustion stability. Instead, it is due to the smaller denominator in Eq.7 (gIMEP) due to overly advanced combustion phasing, i.e., reduced useful work, while the numerator (standard deviation) remained relatively unchanged. At $\phi < 0.425$, a rapid increase in CoV was observed and exceeded the limit because of unstable combustion. RI decreased as combustion was retarded, and the noise criterion was met at ϕ below 0.525 when decreasing the fuel input amount. The RI at maximum efficiency was only 0.3 MW/m^2, which is equivalent to that of a modern SI engine.

Fig. 17 shows the experimental results in which the equivalence ratio for fuel F was fixed at $\phi = 0.5$, and the intake charge temperature was lowered. Fuel A is shown with motoring trace as the dotted line; again, the minimum equivalence ratio for self-sustaining combustion with pure methane was 0.56. When the fuel was changed to F, self-sustaining CI could be achieved not only at T_{in} = 200 °C but also at lower temperatures. Reducing the inlet temperature increased IDT, retarding the start of combustion, and improved the efficiency.

Fig. 18 illustrates the corresponding output parameters from the temperature sweep experiment in Fig. 17, plotted against the intake charge temperature. When the charge temperature was decreased to 170 °C, CoV drastically increased due to misfire, and thus CI combustion was unattainable. Decreasing the temperature to 180 °C was viable (CoV < 0.9%) and retarded CA50, thereby increasing the load. When temperature decreased, the mixture density changed, so additional fuel and air input were required to keep the intake pressure constant. However, gITE was increased despite the increase in fuel and air quantity. As with the previous experiment varying the equivalence ratio, RI decreased significantly to 0.48 W/m^2 when the charge temperature decreased to 180 °C.

The previous results showed that the fuel reactivity improvement through OCM provides flexibility in retarding the combustion (increasing IDT) by reducing either the equivalence ratio or intake temperature, and thereby enhanced system thermal efficiency. It is

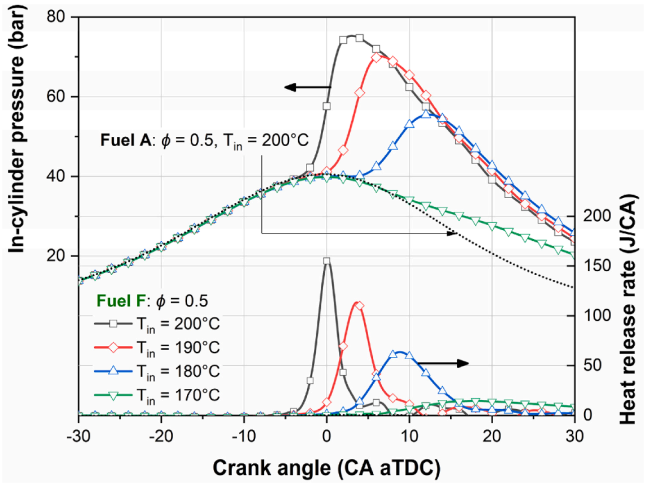

Fig. 17. In-cylinder pressure and HRR with variation in intake charge temperature in CI combustion using fuel F at $\phi = 0.5$ and P_{in} = 1 bar.

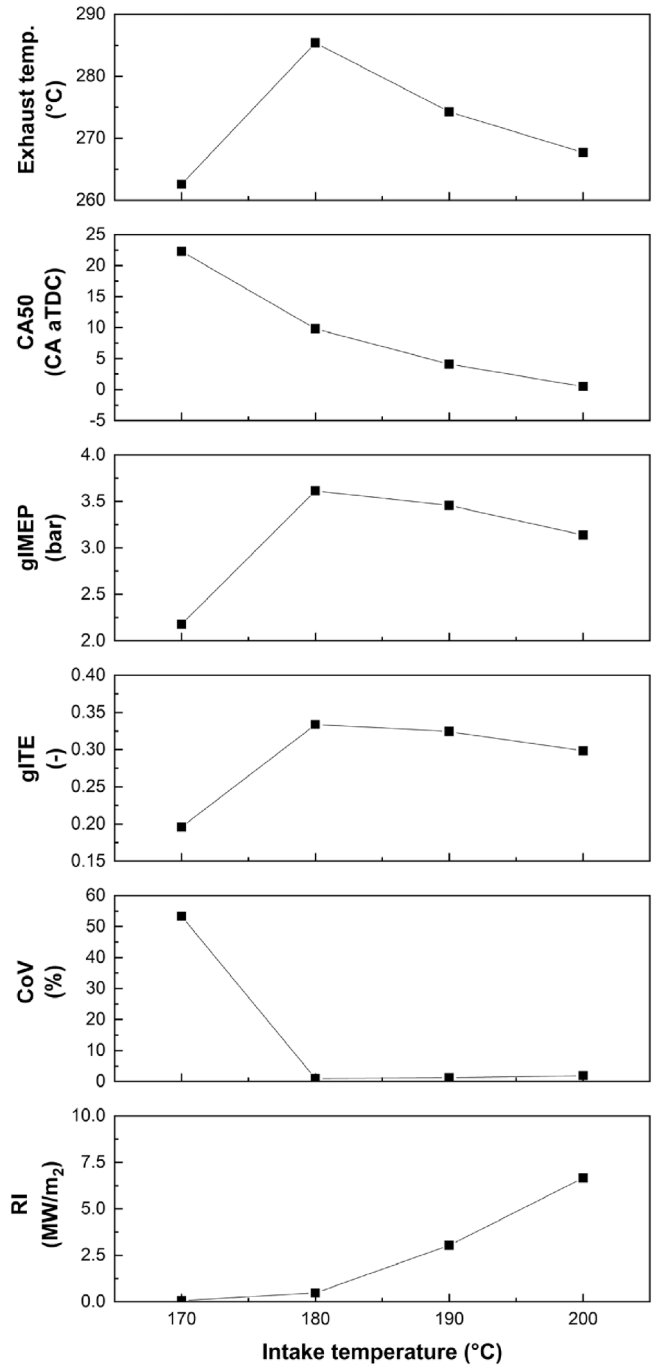

Fig. 18. Engine experimental results for CI combustion with variation in intake charge temperature using fuel F at $\phi = 0.5$ and $P_{in} = 1$ bar: output parameters (exhaust temperature, CA50, gIMEP, gITE, CoV of gIMEP, and RI).

noted that the OCM product has to mix with the fresh air before induction to the combustion chamber in actual application. At this point, the possibility of reducing the intake temperature is particularly meaningful as the actual charge temperature may be limited considering the low enthalpy of OCM products in engine-scale reactors, difficulties in integration, and the feasibility of installing an auxiliary air heater.

Fig. 19 illustrates the feasibility of CI mode depending on the equivalence ratio (vertical axis) and the charge temperature (horizontal axis). Operating points that can achieve stable combustion (CoV < 5%) are indicated by the shaded areas. Some RI values are annotated in the figure. A1 is the area where self-sustaining CI was attainable with fuel A. However, the noise level (RI) here exceeded the limit as explained in

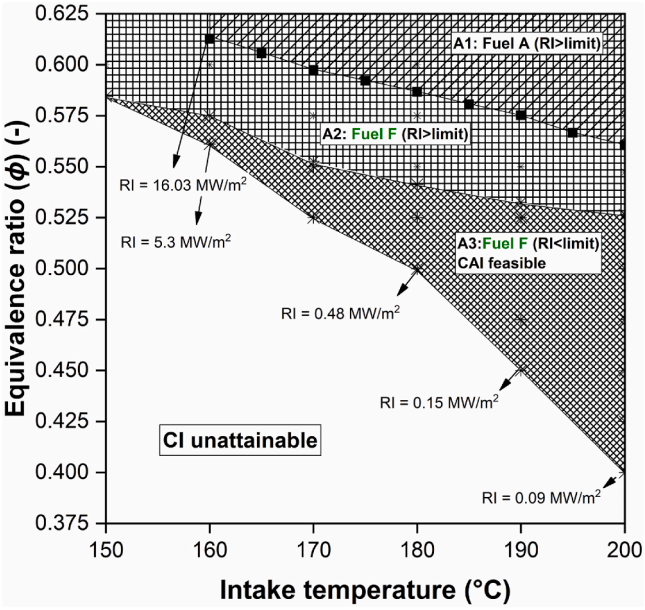

Fig. 19. Comparison of the CI operating range of pure methane (A1, fuel A) and OCM products (A2 and A3, fuel F).

Fig. 13. The lower boundary of A1 corresponds to the minimum equivalence ratio curve in Fig. 13(b). A2 and A3 show the significantly expanded operating range when fuel F is used, by the reactivity enhancement. A3 is an operating range of fuel F that meets the RI constraint, whereas A2 also shows self-sustainable CI, but RI exceeded the limit.

Considerably low CoV and RI were obtained in A3. Anecdotally, arbitrary variation of the equivalence ratio and temperature within the range was enabled with fuel F, without any misfire during the engine operation; the increased reactivity of fuel F gives it high combustion stability and enables CAI. At the low load limit, RI showed remarkably low values with fuel F compared to those of fuel A. A 29.65% of gITE was achieved at $\phi = 0.56$ and $T_{in} = 200$ °C with fuel A. Changing to fuel F at the same equivalence ratio and temperature decreased gITE to 24.2% by overly advanced combustion phasing. However, decreasing the intake temperature to 160 °C led to a remarkable efficiency recovery up to 32.58% by the right-phasing of the combustion. Within the expanded operating range, the maximum thermal efficiency of 32.6% was observed at equivalence ratio of 0.475 and intake temperature of 190 °C, and this is an approximately 9.9% increase in efficiency compared to fuel A (please note that baseline condition exceeds RI limit). Despite the loss in the low heating value of the original fuel by the OCM reaction, the improved reactivity allows lower charge temperature and fuel input, thereby increasing the thermal efficiency by retarding the combustion phasing.

Although a combustion-wise potential of fuel pretreatment using OCM was found in this study, incremental studies are required to answer the remaining questions for applying an OCM reactor to an engine. Unlike studying pellet reactor in this study, optimizing and testing adequate commercial reactor design are needed, as well as packaging and integration into the engine system. Existing heat loss to increase the temperature for catalyst activation needs to be minimized; thermal recuperative design using exhaust gas can also be considered.

4. Conclusion

In this study, OCM was investigated to enhance the reactivity of NG and improve thermal efficiency in internal combustion engines. A comprehensive and systematic approach was taken to fundamentally understand the advantages and disadvantages of OCM modified fuel.

OCM benchtop experiments were employed to confirm methane conversion and production of C_2 species. The impact of the OCM product on laminar flame speed and ignition delay time was studied using computational methods. Experiments in a single-cylinder engine were also carried out in both spark-ignition mode and compression-ignition mode to investigate the effect of OCM-modified fuel on operating range and thermal efficiency. The following conclusions can be drawn from the presented work:

1. The OCM benchtop experiment using a packed bed reactor showed a C_2 yield of 10.8 % at C/O = 6 and a relatively low temperature of 600 °C, demonstrating that a considerable amount of methane can be converted to higher-reactivity hydrocarbons.
2. Based on the obtained fuel blend from the benchtop experiment, the numerical simulation showed the decreased laminar flame speed of OCM-modified fuel due to the byproducts and diluents species. On the other hand, ignition delay time was reduced by the presence of C2 species in the OCM product, despite other species having a prolongation effect.
3. Engine experiments revealed that the OCM products are detrimental to thermal efficiency in spark-ignition mode due to prolonged combustion duration caused by less reactive OCM reaction products. By contrast, in a lean-burn compression-ignition mode, the OCM-modified fuel allowed 9.9% greater system indicated thermal efficiency. In addition, a significantly expanded, controllable operating range with high combustion stability and low noise was obtained.
4. This work showed that OCM products at low concentration (~3% C_2 species by volume) in the fuel mixture can expand the operating range of premixed compression-ignition combustion mode, potentially improving engine thermal efficiency. Future work should involve a broader range of engine operating conditions and the integration of practical OCM reactors with engines. Assessment and minimization of energy loss by heat addition for catalyst activation should be included.

CRediT authorship contribution statement

Seokwon Cho: Conceptualization, Methodology, Validation, Writing – original draft, Investigation, Visualization, Writing – review & editing. **Hyewon Lee:** Conceptualization, Methodology, Validation, Writing – original draft, Investigation, Visualization, Writing – review & editing. **Ying Lin:** Conceptualization, Investigation, Visualization, Data curation. **Satbir Singh:** Conceptualization, Methodology, Supervision, Project administration, Writing – review & editing. **William F. Northrop:** Conceptualization, Methodology, Supervision, Project administration, Writing – review & editing, Funding acquisition.

Declaration of Competing Interest

The authors declare the following financial interests/personal relationships which may be considered as potential competing interests: William F. Northrop reports financial support was provided by US Department of Energy.

Data availability

Data will be made available on request.

Acknowledgments

This material is based upon work supported by the U.S. Department of Energy's Office of Energy Efficiency and Renewable Energy (EERE) under Award Number DE-EE0008333. The authors would also like to acknowledge Daniel Olsen at Colorado State University for providing the ARIES82 mechanism for use in the modeling presented in this paper. Pinaki Pal from Argonne National Laboratory is also acknowledged for providing the 3D CFD mesh and CAD model used to validate experimental data.

References

[1] Korakianitis T, Namasivayam AM, Crookes RJ. Natural-gas fueled spark-ignition (SI) and compression-ignition (CI) engine performance and emissions. Prog Energy Combust Sci 2011;37:89–112. https://doi.org/10.1016/j.pecs.2010.04.002.
[2] United States Energy Information Administration (EIA). Annual Energy Outlook. 2021. n.d. https://www.eia.gov/outlooks/aeo/(accessed December 6, 2021).
[3] Rajasegar R, Niki Y, García-Oliver JM, Li Z, Musculus MPB. Fundamental insights on ignition and combustion of natural gas in an active fueled pre-chamber spark-ignition system. Combust Flame 2021;232:111561. https://doi.org/10.1016/J.COMBUSTFLAME.2021.111561.
[4] Chala GT, Abd Aziz AR, Hagos FY. Natural Gas Engine Technologies: Challenges and Energy Sustainability Issue. Energies (Basel). 2018. 11. https://doi.org/10.3390/en11112934.
[5] Cho H, He B-Q. Spark ignition natural gas engines—A review. Energy Convers Manage 2007;48:608–18. https://doi.org/10.1016/j.enconman.2006.05.023.
[6] Song J, Choi M, Kim D, Park S. Combustion Characteristics of Methane Direct Injection Engine Under Various Injection Timings and Injection Pressures. J Eng Gas Turbines Power 2017;139. https://doi.org/10.1115/1.4035817.
[7] Zeng Ke, Huang Z, Liu B, Liu L, Jiang D, Ren Yi, et al. Combustion characteristics of a direct-injection natural gas engine under various fuel injection timings. Appl Therm Eng 2006;26(8-9):806–13.
[8] Kalam MA, Masjuki HH. An experimental investigation of high performance natural gas engine with direct injection. Energy 2011;36:3563–71. https://doi.org/10.1016/j.energy.2011.03.066.
[9] Wei H, Zhang R, Chen L, Pan J, Wang X. Effects of high ignition energy on lean combustion characteristics of natural gas using an optical engine with a high compression ratio. Energy 2021;223:120053. https://doi.org/10.1016/j.energy.2021.120053.
[10] Kim J, Scarcelli R, Som S, Shah A, Biruduganti MS, Longman DE. Numerical investigation of a fueled pre-chamber spark-ignition natural gas engine. International Journal of Engine Research 2021. 14680874211020180. https://doi.org/10.1177/14680874211020180.
[11] Olsson J-O, Tunestål P, Johansson B, Fiveland S, Agama R, Willi M. Compression Ratio Influence on Maximum Load of a Natural Gas Fueled HCCI Engine. SAE 2002 World Congress & Exhibition, SAE. International 2002. https://doi.org/10.4271/2002-01-0111.
[12] Evans RL. Extending the Lean Limit of Natural-Gas Engines. J Eng Gas Turbines Power 2009;131. https://doi.org/10.1115/1.3043814.
[13] Abbasi Atibeh P, Brear MJ, Dennis PA, Orbaiz PJ, Watson HC. Lean Limit Combustion Analysis for a Spark Ignition Natural Gas Internal Combustion Engine. Combust Sci Technol 2013;185:1151–68. https://doi.org/10.1080/00102202.2013.769785.
[14] Mello P, Pelliza G, Cataluña R, da Silva R. Evaluation of the maximum horsepower of vehicles converted for use with natural gas fuel. Fuel 2006;85:2180–6. https://doi.org/10.1016/j.fuel.2006.04.002.
[15] Ibrahim A, Bari S. An experimental investigation on the use of EGR in a supercharged natural gas SI engine. Fuel 2010;89:1721–30. https://doi.org/10.1016/j.fuel.2009.07.005.
[16] Sen AK, Ash SK, Huang B, Huang Z. Effect of exhaust gas recirculation on the cycle-to-cycle variations in a natural gas spark ignition engine. Appl Therm Eng 2011;31:2247–53. https://doi.org/10.1016/j.applthermaleng.2011.03.018.
[17] Christensen M, Johansson B, Einewall P. Homogeneous Charge Compression Ignition (HCCI) Using Isooctane, Ethanol and Natural Gas – A Comparison with Spark Ignition Operation. International Fuels & Lubricants Meeting & Exposition, SAE. International 1997. https://doi.org/10.4271/972874.
[18] Jun D, Iida N. A Study of High Combustion Efficiency and Low CO Emission in a Natural Gas HCCI Engine. 2004 SAE Fuels & Lubricants Meeting & Exhibition, SAE. International 2004. https://doi.org/10.4271/2004-01-1974.
[19] Kobayashi K, Sako T, Yoshimi Sakaguchi, Morimoto S, Kanematsu S, Suzuki K, et al. Development of HCCI natural gas engines. J Nat Gas Sci Eng 2011;3(5):651–6.
[20] Yap D, Peucheret SM, Megaritis A, Wyszynski ML, Xu H. Natural gas HCCI engine operation with exhaust gas fuel reforming. Int J Hydrogen Energy 2006;31:587–95. https://doi.org/10.1016/j.ijhydene.2005.06.002.
[21] Hariharan D, Yang R, Zhou Y, Gainey B, Mamalis S, Smith RE, et al. Catalytic partial oxidation reformation of diesel, gasoline, and natural gas for use in low temperature combustion engines. Fuel 2019;246:295–307.
[22] Gossler H, Deutschmann O. Numerical optimization and reaction flow analysis of syngas production via partial oxidation of natural gas in internal combustion engines. Int J Hydrogen Energy 2015;40:11046–58. https://doi.org/10.1016/j.ijhydene.2015.06.125.
[23] Banke K, Hegner R, Schröder D, Schulz C, Atakan B, Kaiser SA. Power and syngas production from partial oxidation of fuel-rich methane/DME mixtures in an HCCI engine. Fuel 2019;243:97–103. https://doi.org/10.1016/j.fuel.2019.01.076.
[24] Shudo T, Ono Y, Takahashi T. Ignition Control by DME-Reformed Gas in HCCI Combustion of DME. 2003 JSAE/SAE International Spring Fuels and Lubricants Meeting. SAE International. 2003. https://doi.org/10.4271/2003-01-1824.
[25] Fiore M, Magi V, Viggiano A. Internal combustion engines powered by syngas: A review. Appl Energy 2020;276:115415. https://doi.org/10.1016/j.apenergy.2020.115415.

[26] Lunsford JH. The Catalytic Oxidative Coupling of Methane. Angew Chem, Int Ed Engl 1995;34:970–80. https://doi.org/10.1002/anie.199509701.

[27] Keller GE, Bhasin MM. Synthesis of ethylene via oxidative coupling of methane: I. Determination of active catalysts. J Catal 1982;73:9–19. https://doi.org/10.1016/0021-9517(82)90075-6.

[28] Sun J, Thybaut JW, Marin GB. Microkinetics of methane oxidative coupling. Catal Today 2008;137:90–102. https://doi.org/10.1016/j.cattod.2008.02.026.

[29] Palmer MS, Neurock M, Olken MM. Periodic Density Functional Theory Study of Methane Activation over La2O3: Activity of O2-, O-, O22-, Oxygen Point Defect, and Sr2+-Doped Surface Sites. J Am Chem Soc 2002;124:8452–61. https://doi.org/10.1021/ja0121235.

[30] Kondratenko EV, Peppel T, Seeburg D, Kondratenko VA, Kalevaru N, Martin A, et al. Methane conversion into different hydrocarbons or oxygenates: current status and future perspectives in catalyst development and reactor operation. Catalysis. Science & Technology 2017;7(2):366–81.

[31] Schweer D, Meeczko L, Baerns M. OCM in a fixed-bed reactor: limits and perspectives. Catal Today 1994;21:357–69. https://doi.org/10.1016/0920-5861(94)80157-6.

[32] Sadjadi S, Simon U, Godini HR, Görke O, Schomäcker R, Wozny G. Reactor material and gas dilution effects on the performance of miniplant-scale fluidized-bed reactors for oxidative coupling of methane. Chem Eng J 2015;281:678–87. https://doi.org/10.1016/j.cej.2015.06.079.

[33] Dubois J-L, Cameron CJ. Common features of oxidative coupling of methane cofeed catalysts. Applied Catalysis 1990;67:49–71. https://doi.org/10.1016/S0166-9834(00)84431-0.

[34] Kuś S, Otremba M, Taniewski M. The catalytic performance in oxidative coupling of methane and the surface basicity of La2O3, Nd2O3, ZrO2 and Nb2O5☆. Fuel 2003;82:1331–8. https://doi.org/10.1016/S0016-2361(03)00030-9.

[35] Choudhary VR, Rane VH, Pandit MY. Comparison of Alkali Metal Promoted MgO Catalysts for Their Surface Acidity/Basicity and Catalytic Activity/Selectivity in the Oxidative Coupling of Methane. J Chem Technol Biotechnol 1997;68:177–86. https://doi.org/10.1002/(SICI)1097-4660(199702)68:2<177::AID-JCTB645>3.0.CO;2-U.

[36] Maitra AM. Critical performance evaluation of catalysts and mechanistic implications for oxidative coupling of methane. Appl Catal A 1993;104:11–59. https://doi.org/10.1016/0926-860X(93)80209-9.

[37] Ito T, Wang J, Lin CH, Lunsford JH. Oxidative dimerization of methane over a lithium-promoted magnesium oxide catalyst. J Am Chem Soc 1985;107:5062–8. https://doi.org/10.1021/ja00304a008.

[38] Choudhary VR, Rane VH, Chaudhari ST. Factors influencing activity/selectivity of La-promoted MgO catalyst prepared from La- and Mg- acetates for oxidative coupling of methane. Fuel 2000;79:1487–91. https://doi.org/10.1016/S0016-2361(00)00006-5.

[39] Wang DJ, Rosynek MP, Lunsford JH. Oxidative Coupling of Methane over Oxide-Supported Sodium-Manganese Catalysts. J Catal 1995;155:390–402. https://doi.org/10.1006/jcat.1995.1221.

[40] Pak S, Qiu P, Lunsford JH. Elementary Reactions in the Oxidative Coupling of Methane over Mn/Na2WO4/SiO2and Mn/Na2WO4/MgO Catalysts. J Catal 1998;179:222–30. https://doi.org/10.1006/jcat.1998.2228.

[41] Choudhary VR, Uphade BS, Mulla SAR. Oxidative Coupling of Methane over a Sr-Promoted La2O3 Catalyst Supported on a Low Surface Area Porous Catalyst Carrier. Ind Eng Chem Res 1997;36:3594–601. https://doi.org/10.1021/ie960676w.

[42] DeBoy JM, Hicks RF. The oxidative coupling of methane over alkali, alkaline earth, and rare earth oxides. Ind Eng Chem Res 1988;27:1577–82. https://doi.org/10.1021/ie00081a004.

[43] Choudhary VR, Mulla SAR, Rane VH. Surface basicity and acidity of alkaline earth-promoted La2O3 catalysts and their performance in oxidative coupling of methane. J Chem Technol Biotechnol 1998;72:125–30. https://doi.org/10.1002/(SICI)1097-4660(199806)72:2<125::AID-JCTB880>3.0.CO;2-3.

[44] Sollier BM, Gómez LE, Boix A, v, Miró EE.. Oxidative coupling of methane on Sr/La2O3 catalysts: Improving the catalytic performance using cordierite monoliths and ceramic foams as structured substrates. Appl Catal A 2017;532:65–76. https://doi.org/10.1016/j.apcata.2016.12.018.

[45] Cruellas A, Bakker JJ, van Sint AM, Medrano JA, Gallucci F. Techno-economic analysis of oxidative coupling of methane: Current state of the art and future perspectives. Energy Convers Manage 2019;198:111789. https://doi.org/10.1016/J.ENCONMAN.2019.111789.

[46] Spallina V, Velarde IC, Jimenez JAM, Godini HR, Gallucci F, van Sint AM. Techno-economic assessment of different routes for olefins production through the oxidative coupling of methane (OCM): Advances in benchmark technologies. Energy Convers Manage 2017;154:244–61. https://doi.org/10.1016/J.ENCONMAN.2017.10.061.

[47] Vandewalle LA, van de Vijver R, van Geem KM, Marin GB. The role of mass and heat transfer in the design of novel reactors for oxidative coupling of methane. Chem Eng Sci 2019;198:268–89. https://doi.org/10.1016/j.ces.2018.09.022.

[48] Jašo S, Godini HR, Arellano-Garcia H, Omidkhah M, Wozny G. Analysis of attainable reactor performance for the oxidative methane coupling process. Chem Eng Sci 2010;65:6341–52. https://doi.org/10.1016/j.ces.2010.08.019.

[49] Langille JA, Pasale J, Ren J-Y, Egolfopoulos FN, Tsotsis TT. Ignition enhancement by in situ generated C2 additives for natural gas practical combustor applications. Chem Eng Sci 2004;59:5311–8. https://doi.org/10.1016/j.ces.2004.07.017.

[50] Langille JA, Pasale J, Ren J-Y, Egolfopoulos FN, Tsotsis TT. The use of OCM reactors for ignition enhancement of natural gas combustion for practical applications: Reactor design aspects. Chem Eng Sci 2006;61:6637–45. https://doi.org/10.1016/j.ces.2006.06.017.

[51] Amirante R, Distaso E, Tamburrano P, Reitz RD. Laminar flame speed correlations for methane, ethane, propane and their mixtures, and natural gas and gasoline for spark-ignition engine simulations. Int J Engine Res 2017;18:951–70. https://doi.org/10.1177/1468087417720018.

[52] Dirrenberger P, Le Gall H, Bounaceur R, Herbinet O, Glaude P-A, Konnov A, et al. Measurements of Laminar Flame Velocity for Components of Natural Gas. Energy Fuels 2011;25(9):3875–84.

[53] Ravi S, Sikes TG, Morones A, Keesee CL, Petersen EL. Comparative study on the laminar flame speed enhancement of methane with ethane and ethylene addition. Proc Combust Inst 2015;35:679–86. https://doi.org/10.1016/j.proci.2014.05.130.

[54] Wang Y, Movaghar A, Wang Z, Liu Z, Sun W, Egolfopoulos FN, et al. Laminar flame speeds of methane/air mixtures at engine conditions: Performance of different kinetic models and power-law correlations. Combust Flame 2020;218:101–8.

[55] GRI3.0 Mechanism n.d. http://www.me.berkeley.edu/gri_mech/(accessed July 29, 2019).

[56] Mohr J, Windom B, Olsen DB, Homogeneous MAJ, Delay I. In: Flame Propagation Rate and End-Gas Autoignition Fraction Measurements of Natural Gas and Exhaust Gas Recirculation Blends in a Rapid Compression Machine. American Society of Mechanical Engineers; 2020. https://doi.org/10.1115/ICEF2020-2998.

[57] Zhou C-W, Li Y, Burke U, Banyon C, Somers KP, Ding S, et al. An experimental and chemical kinetic modeling study of 1,3-butadiene combustion: Ignition delay time and laminar flame speed measurements. Combust Flame 2018;197:423–38.

[58] Cantera: An object- oriented software toolkit for chemical kinetics, thermodynamics, and transport processes n.d. http://www.cantera.org (accessed July 29, 2019).

[59] Desantes JM, Bermúdez V, López JJ, López-Pintor D. Sensitivity analysis and validation of a predictive procedure for high and low-temperature ignition delays under engine conditions for n-dodecane using a Rapid Compression-Expansion Machine. Energy Convers Manage 2017;145:64–81. https://doi.org/10.1016/J.ENCONMAN.2017.04.092.

[60] Crossley RW, Dorko EA, Scheller K, Burcat A. The effect of higher alkanes on the ignition of methane-oxygen-argon mixtures in shock waves. Combust Flame 1972;19:373–8. https://doi.org/10.1016/0010-2180(72)90007-7.

[61] Vander molen R, Nicholls JA. Blast Wave Initiation Energy for the Detonation of Methane-Ethane-Air Mixtures. Combust Sci Technol 1979;21(1-2):75–8.

[62] Tan Y, Dagaut P, Cathoinnet M, Boettner J-C. Oxidation and Ignition of Methane-Propane and Methane-Ethane-Propane Mixtures: Experiments and Modeling. Combust Sci Technol 1994;103:133–51. https://doi.org/10.1080/00102209408907691.

[63] Siebers DL, Edwards CF. Autoignition of Methane and Natural Gas in a Simulated Diesel Environment. International Congress & Exposition, SAE. International 1991. https://doi.org/10.4271/910227.

[64] Holton MM, Gokulakrishnan P, Klassen MS, Roby RJ, Jackson GS. Autoignition Delay Time Measurements of Methane, Ethane, and Propane Pure Fuels and Methane-Based Fuel Blends. J Eng Gas Turbines Power 2010;132. https://doi.org/10.1115/1.4000590.

[65] Eubank CS, Rabinowitz MJ, Gardiner WC, Zellner RE. Shock-initiated ignition of natural gas—Air mixtures. Symp (Int) Combust 1981;18(1):1767–74.

[66] Cho S, Busch S, Wu A, Lopez PD. Effect of Fuel Cetane Number on the Performance of Catalyst-Heating Operation in a Medium-duty Diesel Engine. WCX SAE World Congress Experience, SAE. International 2022. https://doi.org/10.4271/2022-01-0483.

[67] Pal P, Kalvakala K, Wu Y, McNenly M, Lapointe S, Whitesides R, et al. In: Numerical Investigation of a Central Fuel Property Hypothesis Under Boosted Spark-Ignition Conditions. American Society of Mechanical Engineers; 2019. https://doi.org/10.1115/ICEF2019-7284.

[68] Pal P, Kolodziej CP, Choi S, Som S, Broatch A, Gomez-Soriano J, et al. Development of a Virtual CFR Engine Model for Knocking Combustion Analysis. SAE Int J Engines 2018;11(6):1069–82.

[69] Eng JA. Characterization of Pressure Waves in HCCI Combustion. SAE Powertrain & Fluid Systems Conference & Exhibition, SAE. International 2002. https://doi.org/10.4271/2002-01-2859.

[70] Lee K, Cho S, Kim N, Min K. A study on combustion control and operating range expansion of gasoline HCCI. Energy 2015;91:1038–48. https://doi.org/10.1016/j.energy.2015.08.031.

[71] Lopez-Pintor D, Dec J, Gentz G. Experimental Evaluation of a Custom Gasoline-Like Blend Designed to Simultaneously Improve ϕ-Sensitivity, RON and Octane Sensitivity. SAE International Journal of Advances and Current Practices in Mobility 2020;2:2196–216. https://doi.org/10.4271/2020-01-1136.

[72] Cho S, Song C, Kim N, Oh S, Han D, Min K. Influence of the wall temperatures of the combustion chamber and intake ports on the charge temperature and knock characteristics in a spark-ignited engine. Appl Therm Eng 2021;182:116000. https://doi.org/10.1016/J.APPLTHERMALENG.2020.116000.

[73] di Sarli V, di Benedetto A. Laminar burning velocity of hydrogen–methane/air premixed flames. Int J Hydrogen Energy 2007;32:637–46. https://doi.org/10.1016/j.ijhydene.2006.05.016.

[74] Halter F, Chauveau C, Gökalp I. Characterization of the effects of hydrogen addition in premixed methane/air flames. Int J Hydrogen Energy 2007;32:2585–92. https://doi.org/10.1016/j.ijhydene.2006.11.033.

[75] Ferris AM, Susa AJ, Davidson DF, Hanson RK. High-temperature laminar flame speed measurements in a shock tube. Combust Flame 2019;205:241–52. https://doi.org/10.1016/j.combustflame.2019.04.007.

[76] Egolfopoulos FN, Law CK. Chain mechanisms in the overall reaction orders in laminar flame propagation. Combust Flame 1990;80:7–16. https://doi.org/10.1016/0010-2180(90)90049-W.

[77] Duva BC, Wang Y-C, Chance L, Toulson E. The Effect of Exhaust Gas Recirculation (EGR) on Fundamental Characteristics of Premixed Methane/Air Flames. WCX SAE World Congress Experience, SAE. International 2020. https://doi.org/10.4271/2020-01-0339.
[78] Zhao H. HCCI and CAI Engines for the Automotive Industry. Elsevier; 2007.
[79] Subramanian G, Pires Da Cruz A, Bounaceur R, Vervisch L. Chemical Impact of CO and H2 Addition on the Auto-ignition Delay of Homogeneous N-heptane/air Mixtures. Combust Sci Technol 2007;179:1937–62. https://doi.org/10.1080/00102200701386065.
[80] Li Z, Cheng X, Wei W, Qiu L, Wu H. Effects of hydrogen addition on laminar flame speeds of methane, ethane and propane: Experimental and numerical analysis. Int J Hydrogen Energy 2017;42:24055–66. https://doi.org/10.1016/j.ijhydene.2017.07.190.
[81] Zeng W, Ma H, Liang Y, Hu E. Experimental and modeling study on effects of N2 and CO2 on ignition characteristics of methane/air mixture. J Adv Res 2015;6:189–201. https://doi.org/10.1016/j.jare.2014.01.003.
[82] Sato S, Yamasaki Y, Kawamura H, Iida N. Research on the Influence of Hydrogen and Carbon Monoxide on Methane HCCI Combustion. JSME Int J, Ser B 2005;48:725–34. https://doi.org/10.1299/jsmeb.48.725.